AALBORG UNIVERSITET

ACTIVE DAMPING OF LCL FILTER RESONANCE IN GRID CONNECTED APPLICATIONS

Master Thesis
by
Anca JULEAN
PED10-1035 - Spring Semester, 2009

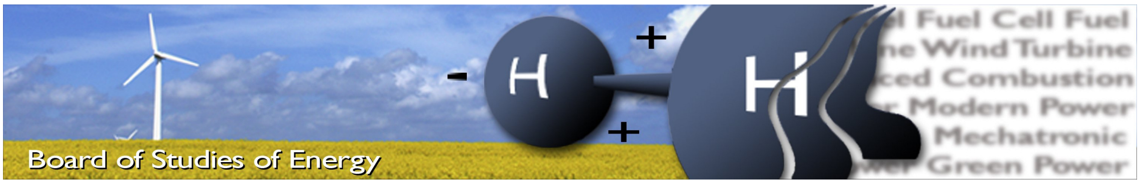

Title:	Active damping of LCL filter resonance in grid connected applications
Semester:	4^{th}
Semester theme:	Master Thesis
Project period:	02.02.09 to 03.06.09
ECTS:	30
Supervisors:	Mihai CIOBOTARU
	Lucian ASIMINOAEI
Project group:	PED4 - 1035

Anca Maria Julean

Copies:	4
Pages, total:	83
Appendix:	2
Supplements:	3 CDs

SYNOPSIS:

The increasing development of renewable energy systems challenges more and more the parameters of their connection to grid. The connection through an LCL filter offers certain advantages, but it brings also the disadvantage of having a resonance frequency.

This project deals with the investigation and the implementation of different methods of active damping of the LCL filter resonance in grid connected applications.

In this project, different active damping methods are be reviewed. The control of the inverter is be implemented, including the synchronization with the grid, the current and dc voltage control loop. Also, different active damping methods are implemented and tested under different conditions.

By signing this document, each member of the group confirms that all participated in the project work and thereby all members are collectively liable for the content of the report.

Preface

The present Master Thesis is conducted at The Institute of Energy Technology. It is written by group 1035 in the 10th semester, during the period from 02.02.2009 to 04.06.2009. The project theme with the title *Active Damping of LCL Filter Resonance in Grid Connected Applications* was chosen from the proposals intended for students from PED 4 semester in collaboration with Danfoss Drives.

Reading Instructions

The bibliography is on page 71. Figures are numbered continuously in their respective chapters. For example figure 2.3 is the third figure in the chapter 2. Equations are numbered in the same way as figures - but they are shown in brackets. Appendices, source codes and documents are attached on a CD-ROM. The contents of the CD-ROM is shown on page 83.

Acknowledgements

The author would like to thank the supervisors Mihai Ciobotaru and Lucian Asiminoaei from Danfoss Drives, for their cooperation and support provided during the project period, through a lot of helpful ideas and suggestions.

Sumary

In the last years, there has been much research in the area of DPGS, as the developement of renewable energy systems has put an increasing demand on the parameters of their connection to the grid. The connection through LCL filters offers certain advantages, but it brings also the disadvantage of having a resonance frequency. This project deals with the study and implementation of some methods through which the resonance frequency of the filter would be actively damped.

The report is structured into eight chapters. In the first chapter, an introduction to the project is made, including a short background, the project motivation and the statement of the goals.

In the second chapter, different damping methods are described shortly. The damping methods of the LCL filter resonance are classified into two classes: passive methods and active methods, both presented with their advantages and disadvantages.

The third chapter deals with the mathematical modeling of the LCL filter and the design of the appropriate values of its components for a power level on 100 kW.

In the forth chapter, the control of the inverter is designed. First part, the PLL is described. Then the current loop is designed, for the case of PI control and the case of P+Resonant control. The last part deals with the design of the dc voltage loop.

The fifth chapter deals with the implementation of two active damping methods: notch filter and virtual resistor. For each of them, the frequency response is studied, as well as the effect of the changes in the grid values and in the filter parameters.

The sixth chapter contains the simulation results that have been obtained using Matlab/Simulink. It is structured into two sections: the first one contains simulation results that confirm the good design of the PI and PR current controllers and of the dc voltage controller. The second one contains simulation results that confirm that active damping has been achieved on the resonance frequency of the LCL filter.

The seventh chapter contains the description of the setup in the laboratory. Moreover, the experimental results, that confirm the simulations, are described and discussed.

The report ends with conclusions and suggestions for future work.

Contents

Introduction

1

1.1 Background

The energy demand has increased in the last years as a result of the industrial development, and is predicted to continue increasing, by at least 50% in the next 10 years. This has focused more research attention on distributed power generation systems like wind turbines, photovoltaic systems, fuel cells, etc. [1]

Fig. 1.1 shows the block diagram of a distributed power generation system (DPGS).

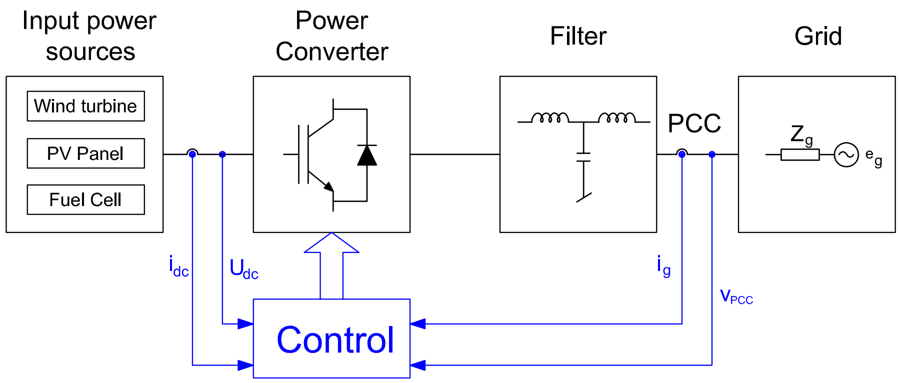

Figure 1.1: *Block diagram of a DPGS.*

The main components of a DPGS are:

- **Input Power Sources:** As shown also in the block diagram, the input power for a DPGS can come from a wind turbine, a photovoltaic panel, a fuel cell or other renewable energy sources. The wind turbine converts the motion of the wind into rotational energy, that can drive an electrical generator. The PV cell is a device that produces electricity when it is exposed to sunlight. The fuel cell is a chemical device, which produces electricity directly, without any intermediate stage. These are the three most used renewable power sources [2],[3].

- **Power Converter:** The most commonly used topology for the power converter is the two-level converter, that consists of six switches. An alternative is the three-level inverter, which contains twice as many transistors. Currently, the interest for multi-level power converters has grown. These converters consist of six or more switches per leg, and the main idea is to create a higher number of output voltage levels, in an attempt to decrease the harmonic content.

- **Filter:** LCL filters have good performances in current ripple attenuations, but they introduce a resonance frequency in the system. Two types of methods are used in order to damp this frequency: passive damping methods and active damping methods.

- **Grid:** A large range of grid impedance values can affect the control of the power converter and, also, can raise new challenges in the design of the filter.
- **Control:** The most used control strategy is the voltage oriented control, but other controls, like the Adaptive Band Hysteresis (ABH) control and Direct Power Control (DPC), are also implemented.

1.2 Project Motivation

In order to reduce the current harmonics around the switching frequency, a large input inductance can be connected in the system. But a big inductance will reduce the system dynamics and the operation range of the converter.[4]

Therefore, instead of using just an inductance, a third order LCL filter can be used with good performances in current ripple attenuation even for small inductances. However, LCL filters bring an undesired resonance effect that generates stability problems. These problems can be solved by using a damping resistor - method called in the literature "passive damping". Although this method has its advantages like reliability and simplicity, it has also disadvantages like increased losses through heat dissipation, which leads to further costs for designing and building a cooling system.

This is the reason why the so-called "active damping methods"have been developed. These methods modify the control algorithm, stabilizing the system without increasing the losses.

The most common active damping methods are:

- virtual resistor
- lead-lag element
- filters

1.3 Problem Formulation

The problem formulation for this project is how to control an inverter connected to the grid through an LCL filter so that the filter resonance would be actively damped.

The block diagram in Fig. 1.1shows the system considered in this project.

The project goals are as follows:

- investigate and review different active damping methods;
- design the LCL filter;
- model and analyze a system with a grid-connected inverter controlled with an active damping method;
- implement an active damping method in the laboratory, using an experimental setup, based on a dSpace control board;

1.4 Project Limitations

The design of the filter and the simulations are carried out on a system with a rated power of 100 kW. However, for the laboratory implementation, a downscaling of the system has been done, due to physical contstraints. The following rating of the system has been used:

- Nominal power: 2.2 kW
- Nominal current: 4.3 A
- Grid voltage: 3x230 V
- DC link voltage: 650 V
- LCL filter components: $L_i = 6.9mH$, $C_f = 4.7\mu F$, $L_g (= L_{transformer}) = 2mH$

1.5 Outline of the project

This project is structured in 8 main chapters:

- **Chapter 1** is an introduction to the project, containing a short background, the project motivation and the goals of the project.
- **Chapter 2** is a brief study of different methods (both passive and active) to achieve damping of the resonance frequency of the LCL filter.
- **Chapter 3** deals with the design of the filter, including the derivation of the transfer function and the calculation of the filter parameters.
- In **Chapter 4**, the design of the control loops is carried out, containing the design of the phase-locked loop, the current loop and the dc voltage loop.
- In **Chapter 5**, two active damping methods (the notch filter and the virtual resistance) are further described and tested in different situations .

- In **Chapter 6**, the simulation of the inverter connected to the grid through an LCL filter is carried out and the results are presented. Also, the active damping of the filter resonance is implemented and the results are discussed.
- **Chapter 7** deals with the description of the test setup and of the results obtained in the laboratory, concerning both the design of the current control and the implementation of active damping.
- **Chapter 8** is the conclusions, which includes also the future work.

Damping Methods of the LCL Filter Resonance 2

In this chapter, different damping methods are described shortly. The damping methods of the LCL filter resonance can be classified into two classes: passive methods and active methods.

2.1 Background

The system considered is the one in Fig. 2.1. The control of the grid-connected inverter is a classical one, with an inner current control loop and an outer voltage control loop, that keeps a constant value of the dc link voltage and provides the reference current for the current loop. Also, a grid synchronization method (phase-locked loop) is used in order to synchronize the control with the phase angle of the grid [5],[2].

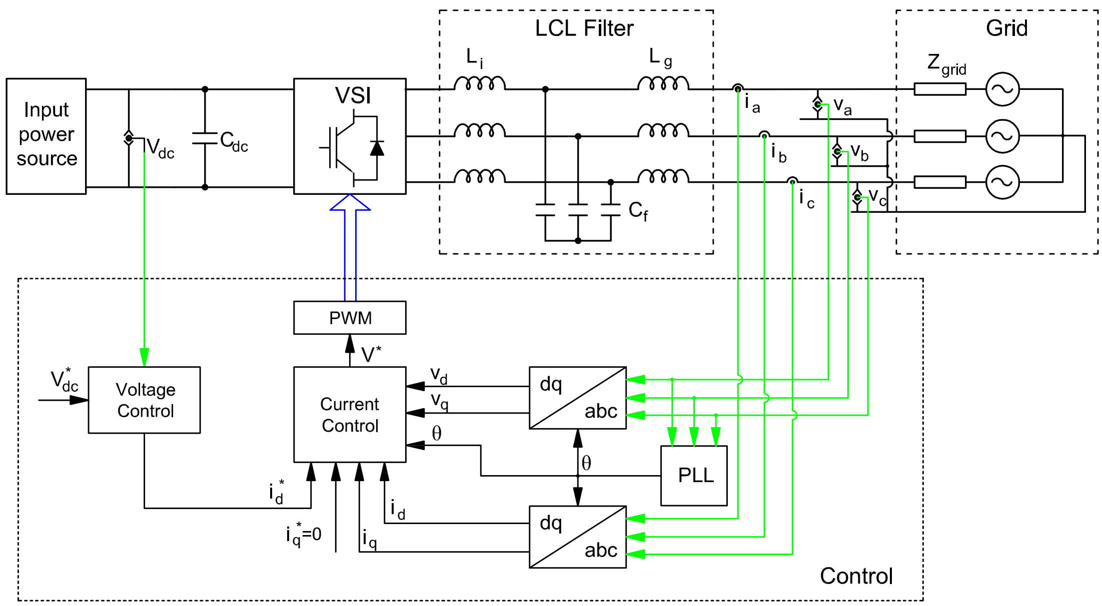

Figure 2.1: *Control of a grid connected VSI.*

2.2 Passive Damping

Passive damping is achieved by adding a resistance in series or in parallel with the capacitance or inductance of the filter. The four possible positions are shown in Fig. 2.2

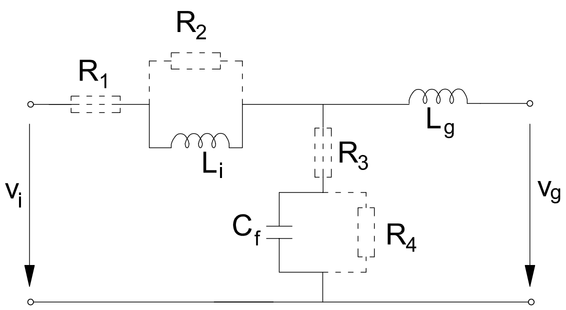

Figure 2.2: *The possible positions for the damping resistance.*

The effects of the damping resistance placed in each of the four positions is shown in Fig. 2.3, as follows:

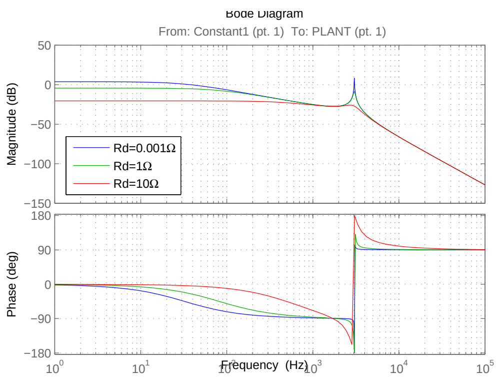

(a) Damping resistance placed in series with the filter inductance.

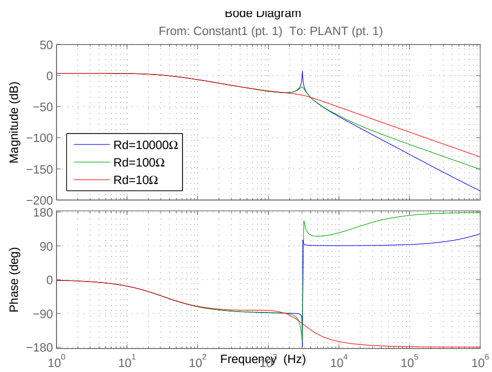

(b) Damping resistance placed in parallel with the filter inductance.

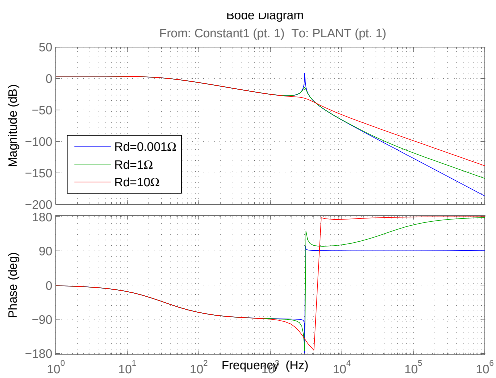

(c) Damping resistance placed in series with the filter capacitance.

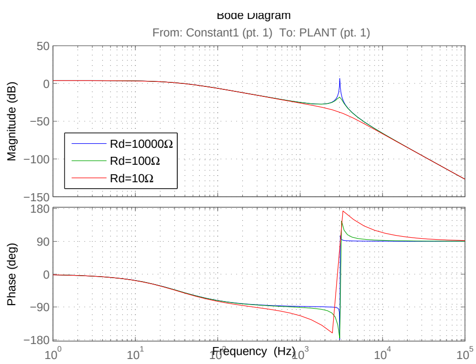

(d) Damping resistance placed in parallel with the filter capacitance.

Figure 2.3: *Bode plots of LCL filter with passive damping.*

The losses on the damping resistance of the LCL filter can be calculated with the formula:

$$P_d = 3 \cdot R_d \cdot \sum_h [i_i(h) - i_g(h)]^2 \tag{2.1}$$

where h is the harmonic order.

2.3 Active Damping

2.3.1 Virtual resistance method

As mentioned before, the resonance frequency of an LCL filter can be damped by connecting a resistor to the filter. But this would greatly reduce the efficiency of the system. If instead of a real resistance, a virtual resistance is used, the transients can be damped with no efficiency losses [6], [7], [8], [9].

The single phase equivalent circuit of the AC side and the block diagram is the one depicted in Fig. 2.4. The current source i_i represents the fundamental component of the phase output current of the VSI and is assumed to be the same as the reference current used in the control loop. Also, v_g is the phase grid voltage.

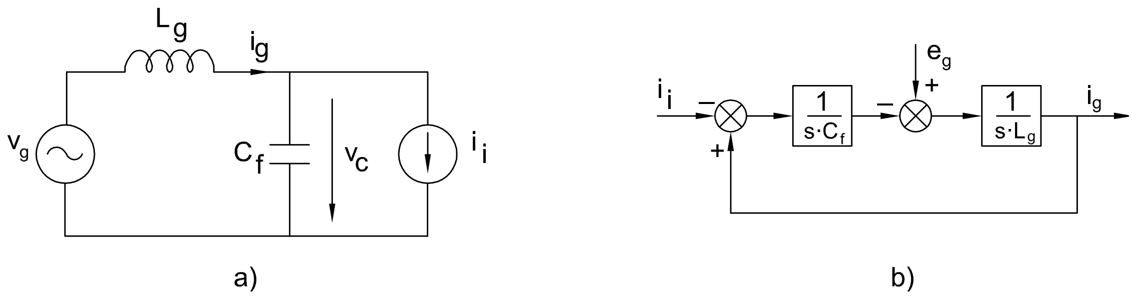

Figure 2.4: *a) Single-phase equivalent circuit of the AC side of the inverter. b) Associated block diagram.*

According to [6], there are four possible topologies concerning the position of the virtual resistor, the same as for the passive damping (Fig. 2.2).

If the virtual resistor is connected in series with the inductance or the capacitance, an additional current sensor is needed and if the virtual resistor is connected in parallel with the inductance or the capacitance, an additional voltage sensor is required.

The concept of the virtual resistance is explained in the following for the first case (virtual resistance connected in series with the filter inductance). For the other cases, the same aproach can be used [7].

As seen in Fig. 2.5.a), the resistor connected in series with the filter inductance has the role of reducing the voltage across this inductance, by a voltage proportional to the current that flows through it. In the control loop, the current through the filter inductance is measured and differentiated by a constant of sC_fR_1. However, a real resistance is not used. The differentiator output is injected in the reference current signal of the converter [6], [7].

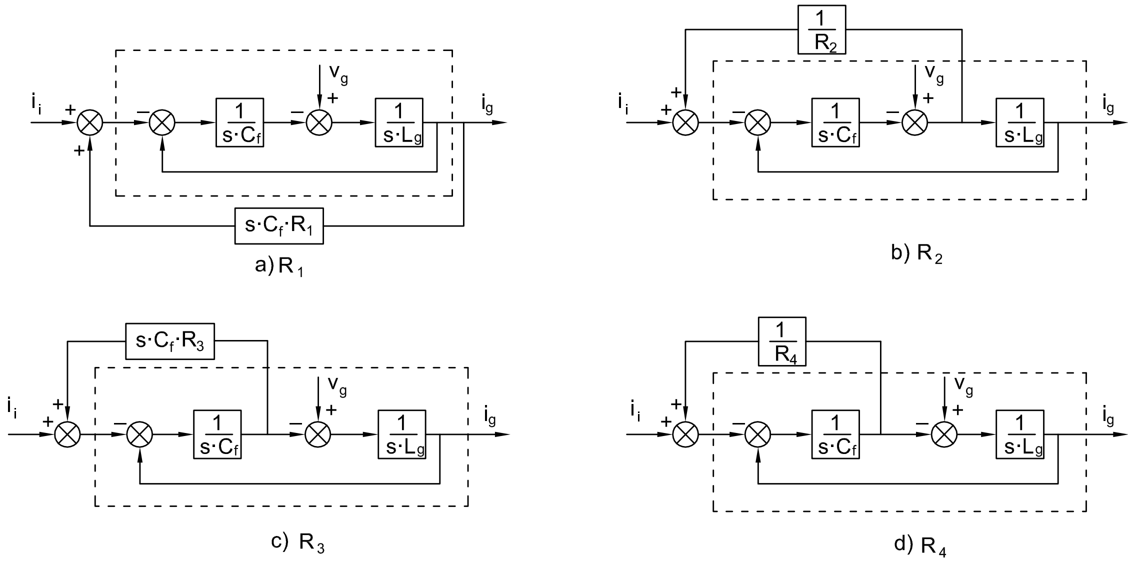

Figure 2.5: *Block diagrams of the system using the virtual resistor method.*

In practice, more virtual resistors can be used at the same time. In the case of using the virtual resistors connected as in Fig. 2.5.a) and b), the diagram of the control loop is the one in Fig. 2.6.

If the virtual resistor is connected in series with the filter inductance or filter capacitance, then the control requires an additional current sensor and a differentiator. The differentiator might bring noise problems as it amplifies high-frequency signals. If the virtual resistor is connected in parallel with the filter inductance or filter capacitance, then the control requires an additional voltage sensor and an amplifier.

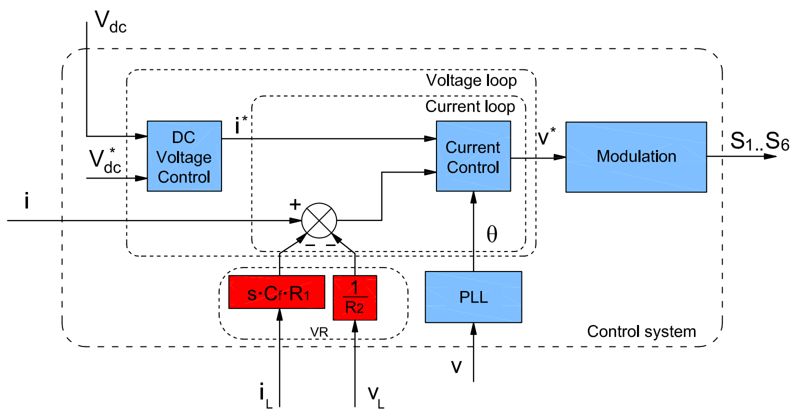

Figure 2.6: *Block diagram of the controller.*

Fig. 2.7 shows a comparison between the Bode Plots of the undamped system and of the system actively damped using a virtual resistor connected in series with the filter capacitance.

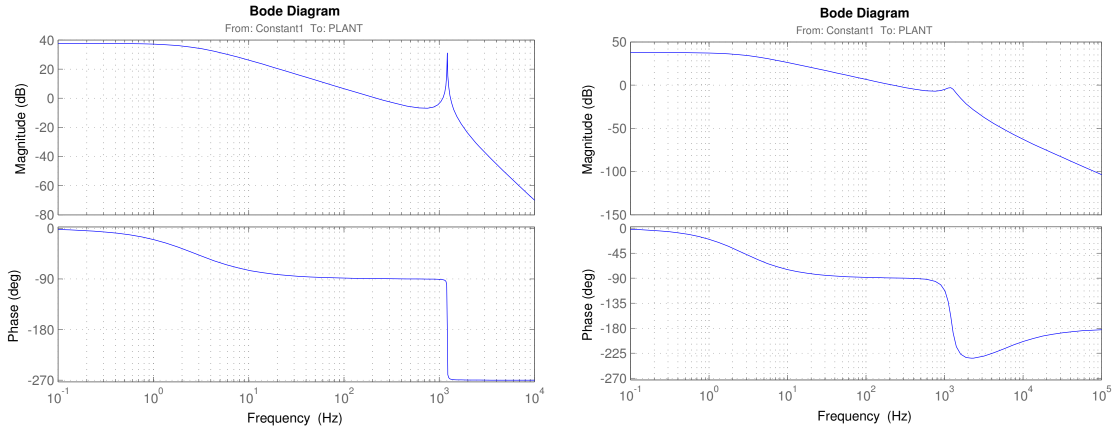

(a) Bode Plot of the undamped system.

(b) Bode Plot of the system actively damped using a virtual resistor

Figure 2.7: *Comparison of Bode Plots.*

2.3.2 Lead-Lag Compensator

The shift in the phase angle introduced by the filter can be compensated with an lead-lag compensator [10],[8]. The lead compensator has the following equation :

$$L(s) = k_d \frac{T_d s + 1}{\alpha T_d s + 1} \tag{2.2}$$

The lead compensator adds positive phase to the system. The compensator needs to be tuned to the resonance frequency of the filter.[8]

Fig. 2.8 shows the Bode Plots of the undamped system, of the lead compensator and of the system actively damped using a lead compensator.

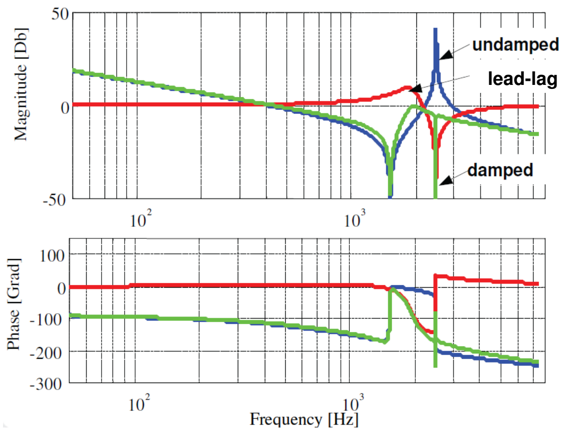

Figure 2.8: *Bode Plot of the system damped using a lead compensator.*

An active damping method using a lead-lag compensator is described in [10]. This method uses a lead-lag element in the synchronous reference frame applied to the feedback from the capacitor voltage (Fig. 2.9).

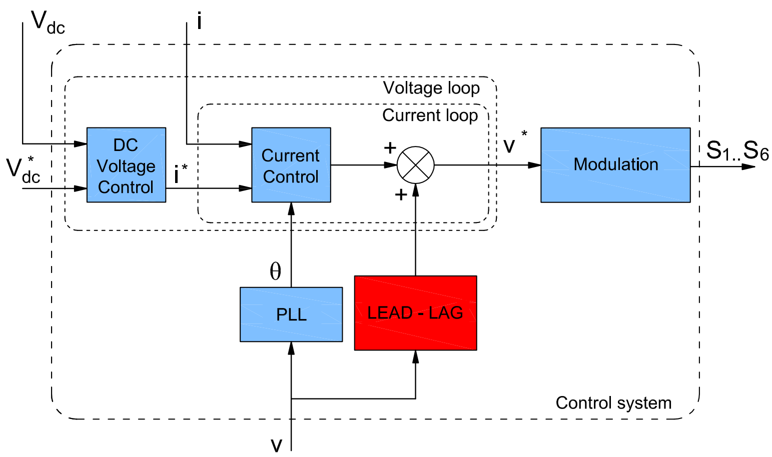

Figure 2.9: *Control system with lead-lag compensator.*

The grid voltages are used both for the grid synchronization and for the active damping. First, they are transformed in the reference frame the controller works with and then inputed to a lead-lag block. Then, the output from the lead-lag block are added to the output of the current regulators and then processed to obtain the duty cycles to be sent to the inverter.

In [8], another active damping method with a lead-lag compensator is proposed, in which the only sensors used are for the output currents and the dc bus voltage, as it can be seen in Fig. 2.10

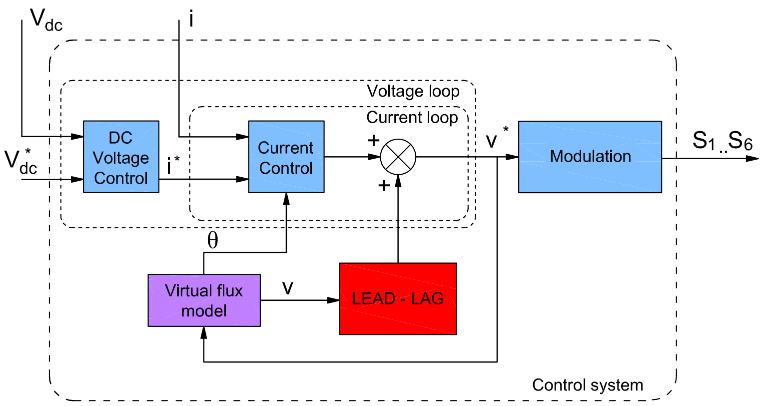

Figure 2.10: *Sensorless control system with lead-lag compensator.*

In this method, the capacitor voltage is estimated with the virtual flux aproach [8]. The signal outputed by the Virtual Flux block is compensated using a Lead-Lag element, and then added to the output of the current controller.

2.3.3 Notch filter

This method consists of adding a filter in series with the reference voltage of the modulator (Fig. 2.11).

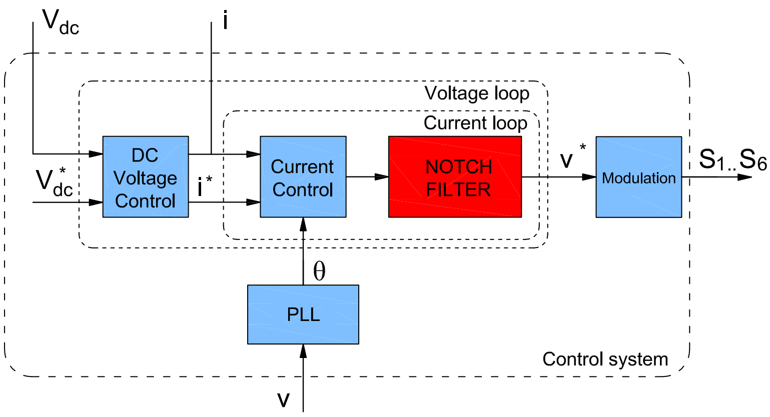

Figure 2.11: *Control system with notch filter.*

The basic idea can be explained in the frequency domain by introducing a negative peak (notch) in the system, that compensates for the resonant peak due to the LCL filter [11]. This can be done by adding a notch filter in the current loop. The frequency of the Notch filter has to be tuned at the resonance frequency of the LCL filter, in order to provide a good damping.

The LCL filter in Fig. 2.12 has a resonance frequency of 4kHz, and the Notch filter introduces a notch at this frequency. This Bode plot shows the the frequency response of the undamped system, of the notch filter and of the system actively damped using a notch filter.

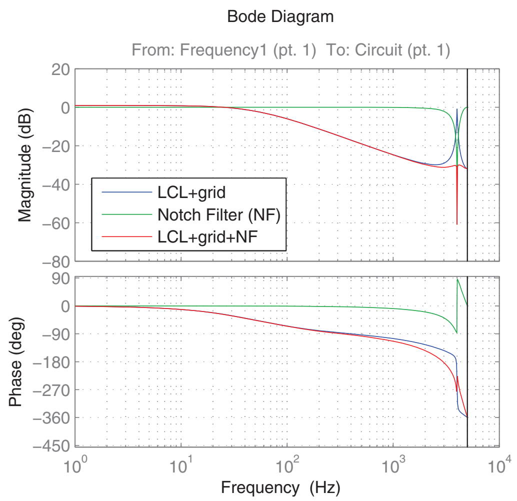

Figure 2.12: *Bode Plot of the system damped a Notch filter[12].*

Filter Design

3

This chapter deals with the mathematical modeling of the LCL filter and the design of the appropriate values of its components for a power level on 100 kW.

3.1 Filter topology

The filters connected to the inverter output have basically a four-pole topology [13], like the one in Fig. 3.1.

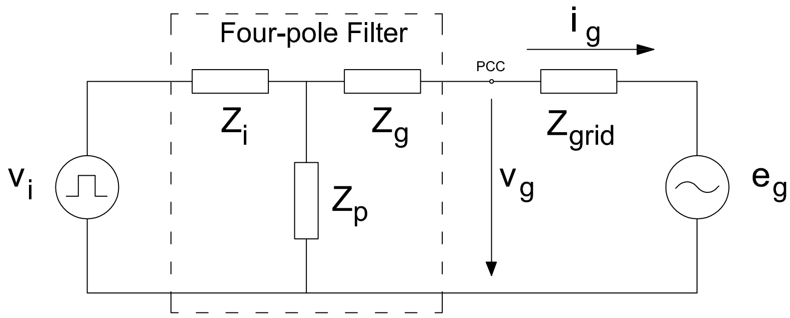

Figure 3.1: *Circuit configuration of a three element filter [13].*

3.1.1 L Filter

In this configuration, Z_i is finite, Z_p is infinite and Z_g=0 (Fig. 3.2), meaning that the filter consists only of an inductance in series with the inverter.

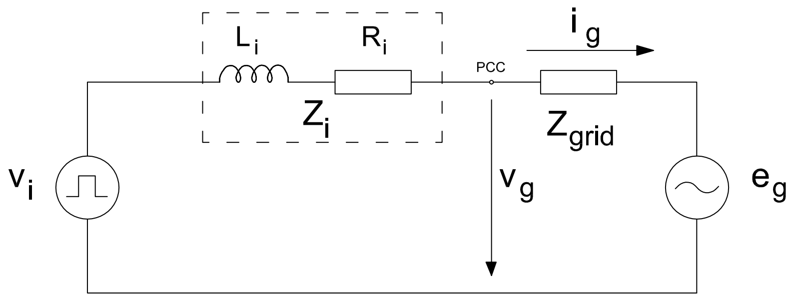

Figure 3.2: *Circuit with L filter.*

One of the disadvantages of this topology, is the poor system dynamics due to the voltage drop on the inductance that causes big response times.

Also, as it can be seen from the Bode plot (Fig. 3.3), in the case of L filters, the damping is increased by $20db/dec$. Therefore, in order to obtain a good damping, a large filter (that can be bulky and expensive) has to be used.

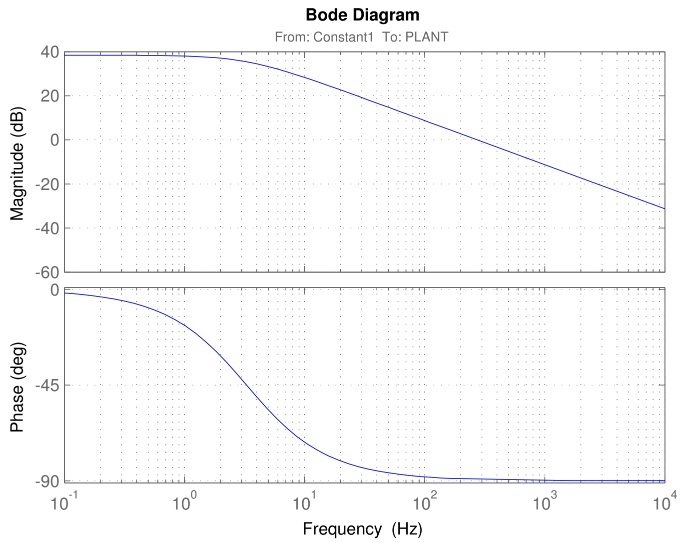

Figure 3.3: *Bode plot of an L Filter.*

3.1.2 LC Filter

In this configuration, Z_i is finite, Z_p is finite and Z_g=0, meaning that the filter consists of an inductance in series with the inverter and a capacitance in parallel (Fig. 3.4). By using this parallel capacitance, the inductance can be reduced, thus reducing costs and losses.

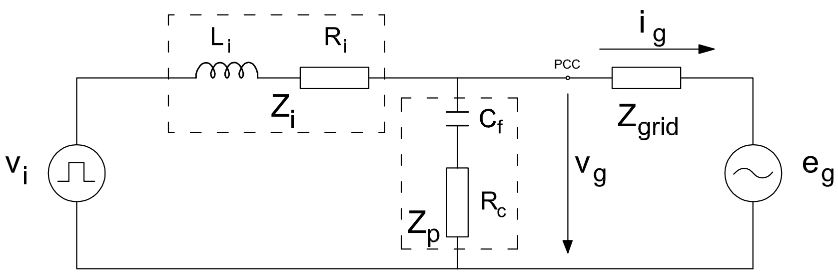

Figure 3.4: *Circuit with LC filter.*

By using a large capacitance, other problems might appear, like high inrush currents, high capacitance current at the fundamental frequency, or dependence of the filter on the grid impedance for overall harmonic attenuation [13].

The Bode plot of the LC filter is shown in Fig. 3.5.

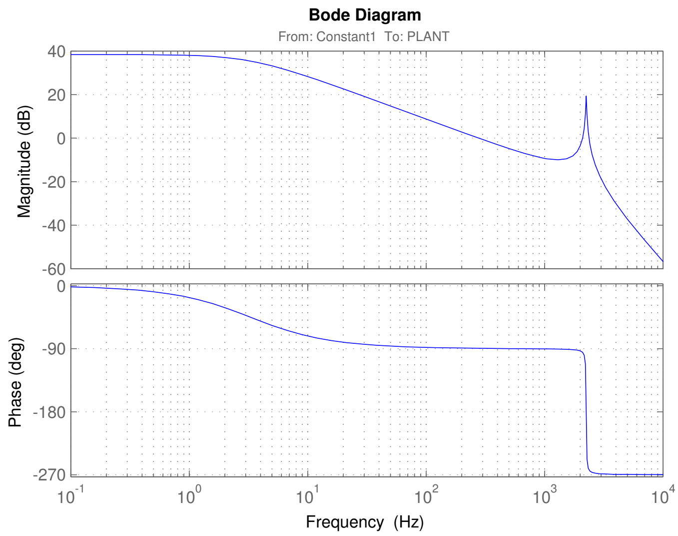

Figure 3.5: *Bode plot of an LC Filter.*

3.1.3 LCL Filter

Like in the case of the LC filter, the increase in the size of the capacitance leads to a reduction in the cost and weight of the filter.

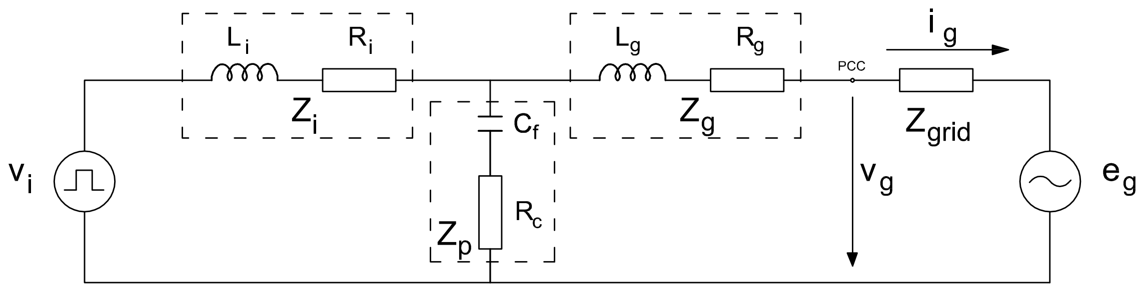

Figure 3.6: *Circuit with LCL filter.*

The LCL filter (Fig. 3.6) brings the advantage of providing a better decoupling between the filter and grid impedance (as it reduces the dependence of the filter on the grid parameters) and a lower ripple of the current stress across the grid inductor [13].

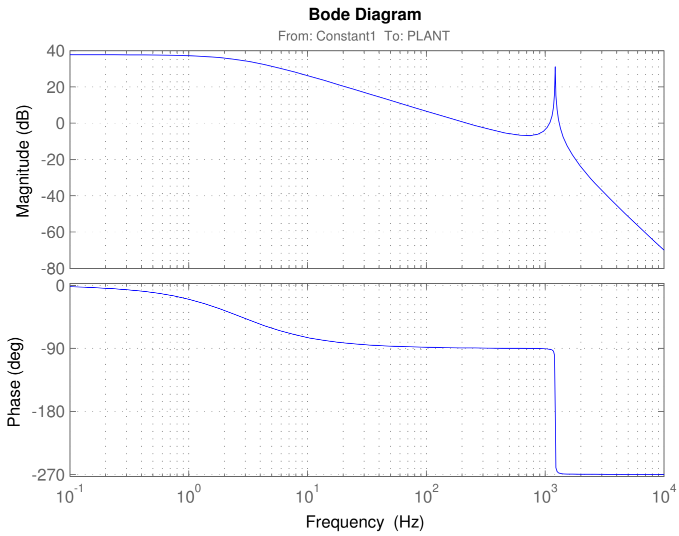

Figure 3.7: *Bode plot of an LCL Filter.*

3.2 Transfer function of the LCL filter

In order to obtain the transfer function of the LCL filter, the one phase electrical diagram in Fig. 3.8 is considered. The components of the filter on each phase are considered to be identical, so the circuit below is suitable for the other two phases.

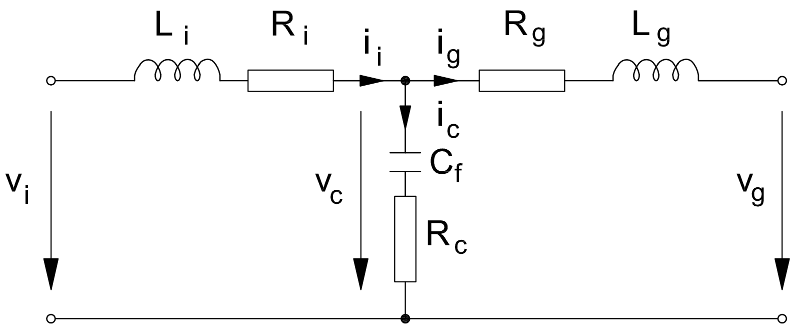

Figure 3.8: *One phase electrical circuit of an LCL filter.*

Using Kirchoff's laws, the filter model in s-plane can be written with the following equations:

$$i_i - i_c - i_g = 0 \tag{3.1}$$

$$v_i - v_c = i_i(sL_i + R_i) \tag{3.2}$$

$$v_c - v_g = i_g(sL_g + R_g) \tag{3.3}$$

$$v_c = i_c(\frac{1}{sC_f} + R_i) \tag{3.4}$$

The following notations have been made:

- v_i inverter voltage
- i_i inverter current
- v_c voltage drop on filter capacitance
- i_c current accross filter capacitance
- v_g grid voltage
- i_g grid current
- L_i filter inductance on inverter side
- R_i inverter side parasitic resistance
- C_f filter capacitance
- R_c parasitic resistance of filter capacitance
- L_g filter inductance in grid side
- R_g grid side parasitic resistance

The block diagram of the filter is shown in Fig. 3.9

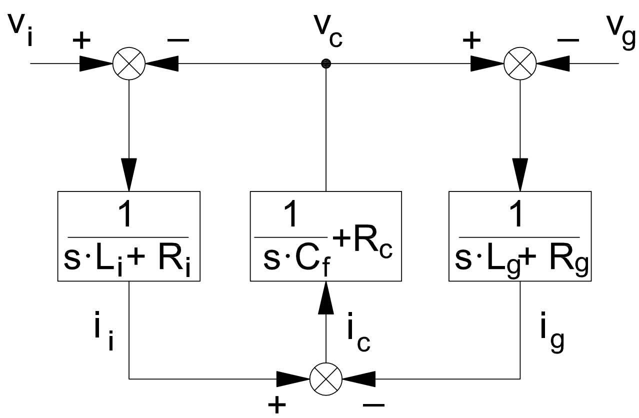

Figure 3.9: *Block diagram an LCL filter.*

The transfer function of the filter is expressed by:

$$H_{LCL} = \frac{i_g}{v_i} \tag{3.5}$$

In order to compute the transfer function of the filter, some mathematical calculations have to be made. The grid voltage is assumed to be an ideal voltage source and it represents a short circuit for harmonic frequencies, and for the filter analysis it is set to zero: $v_g = 0$.

From the equations (3.3) and (3.4), the following relation can be written:

$$i_g(sL_g + R_g) = i_c(\frac{1}{sC_f} + R_c) \Rightarrow i_c = i_g \frac{s^2 C_f L_g + sC_f R_g}{sC_f R_c + 1} \tag{3.6}$$

Equation (3.2) can be written as:

$$v_i = v_c + i_i(sL_i + R_i) \tag{3.7}$$

By introducing (3.3), (3.1) and (3.6) into the above relation, the inverter voltage can be written as:

$$v_i = i_g(sL_g+R_g)+(i_g+i_c)(sL_i+R_i) = i_g(sL_g+R_g)+(i_g+i_g\frac{s^2 C_f L_g + sC_f R_g}{sC_f R_c + 1})(sL_i+R_i) \tag{3.8}$$

$$\Rightarrow v_i = i_g(sL_g + R_g + sL_i + R_i + \frac{(sL_i + R_i)(s^2 C_f L_g + sC_f R_g)}{sC_f R_c + 1}) \tag{3.9}$$

So, considering (3.5), the transfer function of the filter can be calculated as:

$$H = \frac{sR_c C_f + 1}{s^3 L_g L_i C_f + s^2 C_f(L_g(R_c + R_i) + L_i(R_c + R_g)) + s(L_g + L_i + C_f(R_c R_g + R_c R_i + R_g R_i)) + R_g + R_i} \tag{3.10}$$

3.3 Requirements concerning the power delivered to the grid

When studying the grid compatibility of a device, the following issues need to be addressed: average and maximum power produced, reactive power level, grid short-circuit current (weak or stiff grid conditions), voltage fluctuations, coupling procedure to the grid, flicker and harmonics[14].

The *IEEE Standard 519-1992*[14] provides a table which presents the limits for the total harmonic distortion (THD) of the currents, for a voltage level of below 69kV.

Maximum Harmonic Current Distortion in Percent of I_L **Individual Harmonic Order (Odd Harmonics)**						
I_{sc}/I_L	< 11	$11 \leq h < 17$	$17 \leq h < 23$	$23 \leq h < 25$	$35 \leq h$	TDD
< 20	4.0	2.0	1.5	0.6	0.3	5.0
$20 < 50$	7.0	3.5	2.5	1.0	0.5	8.0
$50 < 100$	10.0	4.5	4.0	1.5	0.7	12.0
$100 < 1000$	12.0	5.5	5.0	2.0	1.0	15.0
> 1000	15.0	7.0	6.0	2.5	1.4	20
Even harmonics are limited to 25% of the odd harmonics limits above.						

Table 3.1: *Current distortion Limits for GEneral Dist. Systems (120V - 69 000V)[14]*

The ratio I_{sc}/I_L is the ratio of the short-circuit current available at the point of common coupling (PCC), to the maximum fundamental load current.

The limits listed in the table above have been calculated for six-pulse rectifiers so, when converters with another number of pulses (q) are used, the limits of the harmonic orders are increased by a factor of $\sqrt{q/6}$ [14].

3.4 Limits on the filter parameters

In the technical litarature there are many suggestions that may be considered designing an LCL filter [15],[13],[16],but there is no designated step-by-step strategy on this matter. However, in this project the following limitations on the filter parameters have been taken into account [15]:

- the value of the capacitance is limited by the decrease of the power factor, that has to be less than 5% at the rated power;
- the total value of the filter inductance has to be less than 0.1 p.u. for low power filters. However, for high power levels, the main aim is to avoid the saturation of the inductors;
- the resonance frequency of the filter should be higher than 10 times the grid frequency and than half of the switching frequency.

3.5 Calculation of the filter values

The system parameters considered for the calculation of the filter components, for a power level of 100kVA, are presented in the table bellow.

Grid Line to Line Voltage	E_n = 380V
Output Power of the Inverter	S_n = 100kVA
DC-Link Voltage	V_{dc} = 650V
Frequency of grid voltage	f = 50Hz
Switching frequency	f_{sw} = 3kHz

Table 3.2: *Parameters of the considered system.*

For the further development, the base values are calculated, as the filter values are reported as a percentage of these.

$$Z_b = \frac{(E_n)^2}{S_n} = 1.444[\Omega] \tag{3.11}$$

$$L_b = \frac{Z_b}{\omega_n} = 4.596[mH] \tag{3.12}$$

$$C_b = \frac{1}{\omega_n Z_b} = 2204.3621[\mu F] \tag{3.13}$$

The first step is to design the inverter side inductance, which is determined by [15]:

$$\frac{i_i(n_{sw})}{v_i(n_{sw})} \approx \frac{1}{\omega_{sw} L_i} \tag{3.14}$$

where ω_{sw} is the switching frequency and n_{sw} is the frequency multiple of the fundamental frequency at the switching frequency.

According to equation (3.14), a current ripple on the inverter side of 1% is obtained with an inductance $L_i = 530\mu H(11.53\%)$.

A filter capacitance $C_f = 110\mu F$ fulfills the requirement on the power factor stated before.

A ripple attenuation of 20% is selected on the grid side with respect to the current ripple on the inverter side. The dependency of the ripple attenuation to the inductance ration is depicted in Fig. 3.10

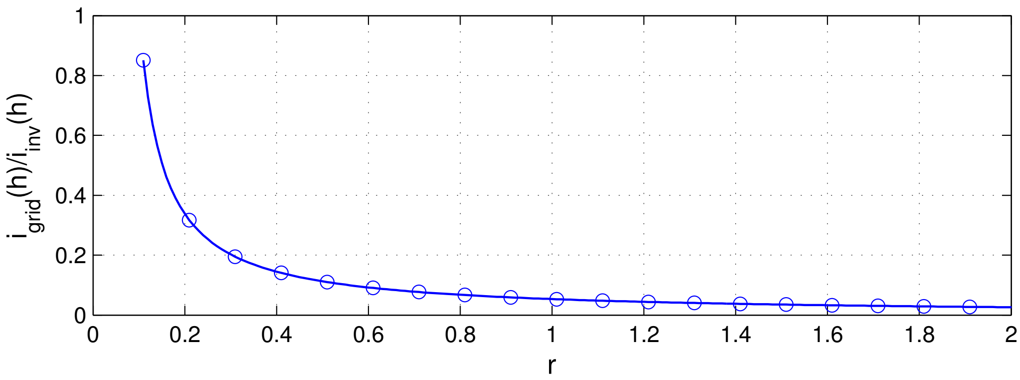

Figure 3.10: *Current ripple attenuation as a function of the inductance ratio for 100kVA.*

The ripple attenuation of 20% is obtained with a ratio of $r = 0.32$. This means that the grid side inductance L_g is equal to $r \cdot L_i \approx 170\mu H(3.69\%)$.

Having chosen the filter values, the resonance frequency of the filter can be calculated as:

$$\omega_{res} = \sqrt{\frac{L_i + L_g}{L_i \cdot L_g \cdot C_f}} = 14.97 \cdot 10^3 \Rightarrow f_{res} = 1.337[kHz] \tag{3.15}$$

The zero-pole map in Fig. 3.11 and the Bode plot of the designed filter is depicted in Fig. 3.12 and .

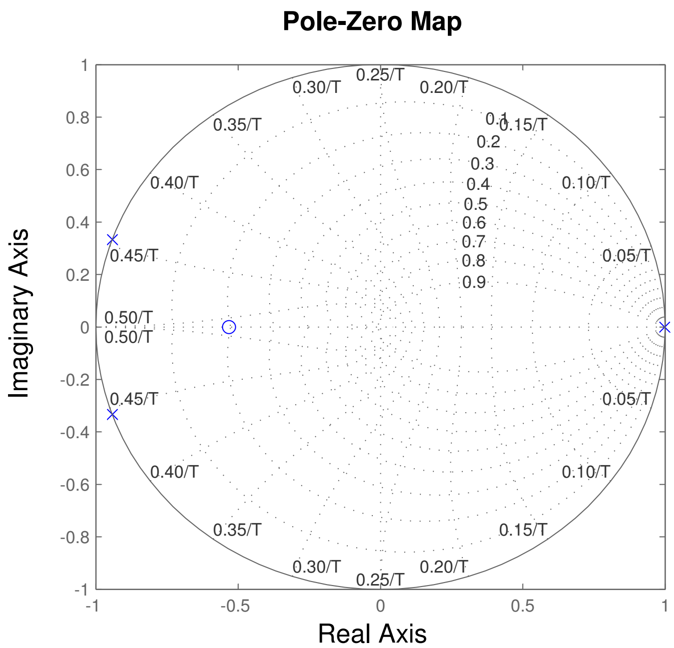

Figure 3.11: *Zero-Pole Map of the LCL filter for a power level of 100kVA.*

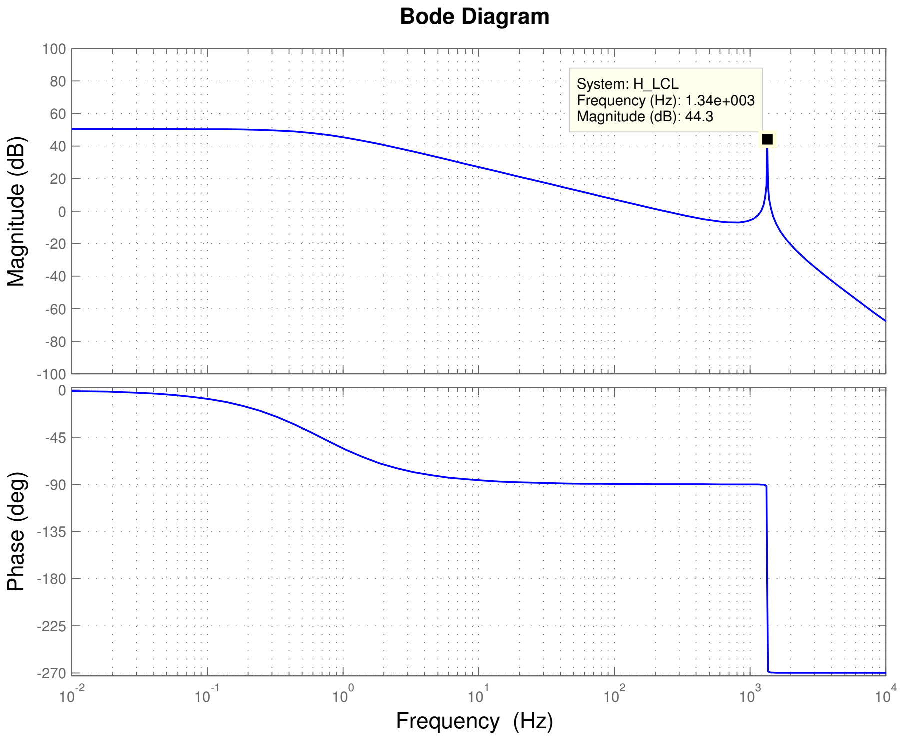

Figure 3.12: *Bode plot of the designed LCL filer for a power lever of 100kVA.*

3.6 Sampling frequency selection

An issue that needs to be considered before begining to design the control of the system, is to choose the optimal sampling frequency of the control system. The low resonance frequency of the filter imposes some limits on the range of sampling frequencies of the control.

Fig. 3.13 show the root loci of the open loop PI current control, plotted at different sampling frequencies. As it can be seen, if a sampling frequency f_s of 2000Hz is chosen, the system is always unstable, as the resonance poles given by the filter are always out of the unity circle.

In the case of $f_s = 3000Hz$ to $f_s = 4000Hz$, the system is stable for a large range of K_p. As the sampling frequency increases, the system remains stable for a lower and lower range of K_p, as it is the case with the sampling frequency of 5000Hz.

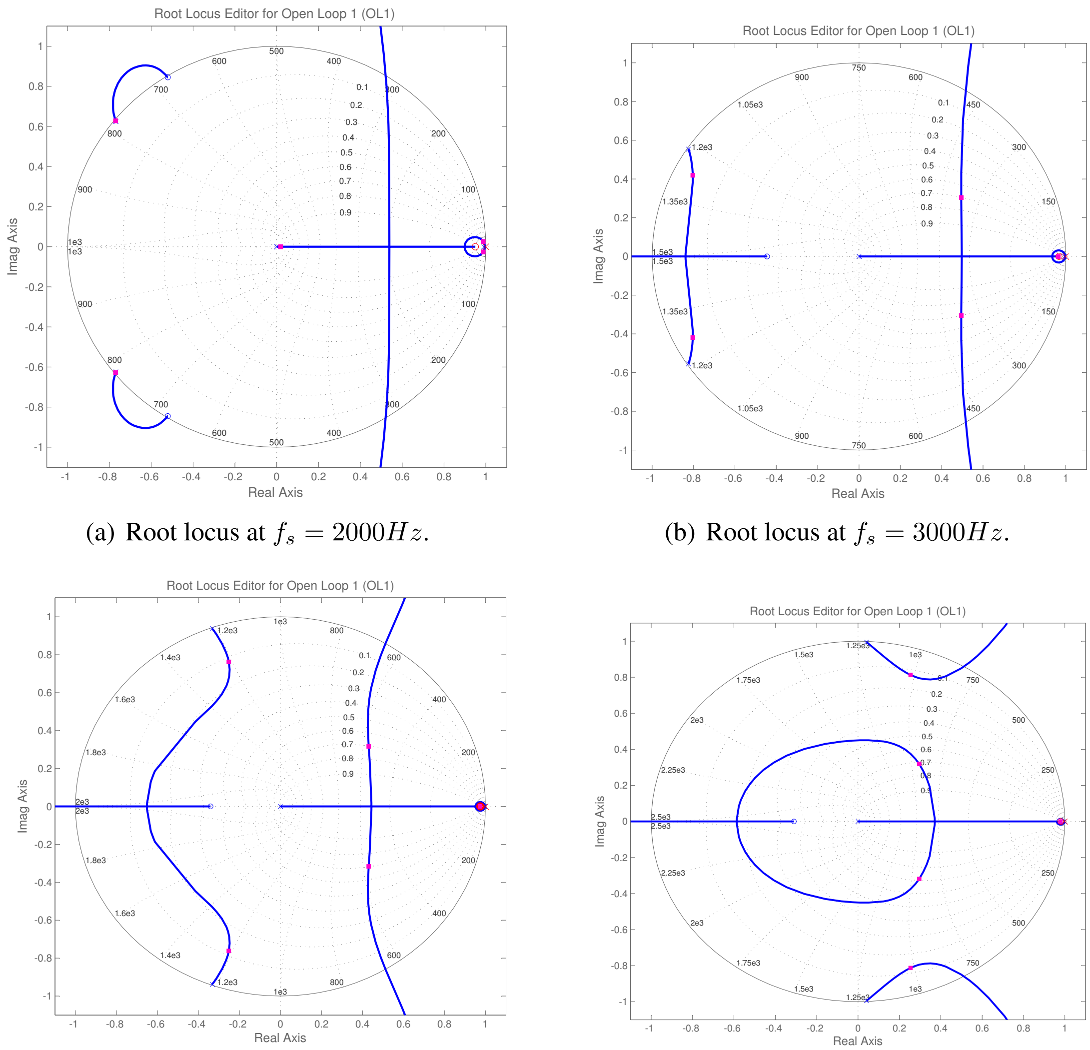

(a) Root locus at $f_s = 2000Hz$.

(b) Root locus at $f_s = 3000Hz$.

(c) Root locus at $f_s = 4000Hz$.

(d) Root locus at $f_s = 5000Hz$.

Figure 3.13: *Root loci of the open loop current control.*

The sampling frequency chosen for this project in order to tune the parameters of the controller is 3000Hz.

Control Design

4

In this chapter, the control of the inverter is designed. In the first part, the PLL is described. Then the current loop is designed, for the case of PI control and the case of P+Resonant control. The last part deals with the design of the dc voltage loop.

The block diagram of the inverter control considered in this project is presented in Fig. 4.1.

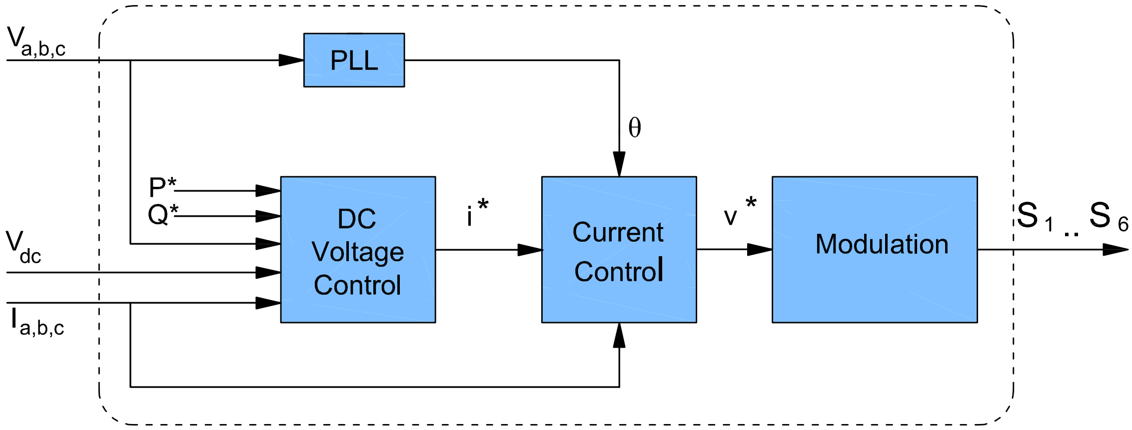

Figure 4.1: *Control block diagram of the grid connected-system.*

The current is oriented along the active voltage component (V_d), this is why this strategy is called voltage oriented control. A PLL alogithm detects the phase angle of the grid, the grid frequency and the grid voltage. The frequency and the voltage are needed for monitoring the grid conditions and for complying with the control requirements. The phase angle of the grid is required for reference frame transformations.

If a PI current control is implemented, then the currents are transformed into the synchronous reference frame, and the algorithm implements also the decoupling between the two axes. If a P+Resonant controller is used, then the currents are transformed into the stationary reference frame and decoupling is not implemented.

For the dc voltage control, a standard PI controller is used also for the DC voltage and it outputs the reference for the current control [17].

The modulation block calculates the propper states of the switches in order to obtain the reference input voltage.

4.1 Phase-Locked-Loop (PLL)

When dealing with the control of grid connected converters, an aspect that needs to be taken into account is the correct generation of the reference signals, which is obtained with a fast and accurate detection of the phase angle and the grid frequency and voltage. One of the methods to synchronize the reference current of the inverter with the grid voltage, is an algorithm called Phase-Locked-Loop (PLL).

The PLL can be defined as an algorithm that determines a signal to track another, so that the output signal is synchronized with the input one both in frequency and in phase [18],[19]. A common way to realize the PLL is in the 'dq' reference frame.

The block diagram of the PLL algorithm implemented in the synchronous reference frame, is shownin Fig. 4.2.

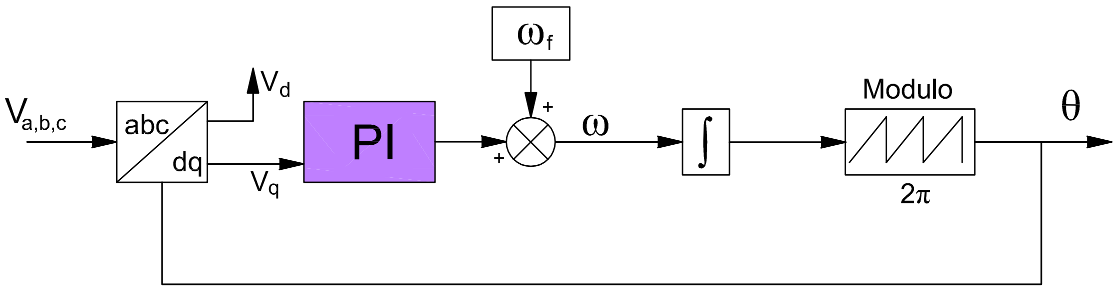

Figure 4.2: *Block diagram of PLL.*

The algorithm uses as input the measured grid voltage, and performs an $abc - dq$ transformation. The 'phase-lock' is realised by setting V_q to 0, using a PI controller. The output of the PI controller is the grid frequency, which, when added to the feed-forward frequency and integrated, provides the grid phase angle, θ. A modulo division block is used to aviod θ from getting too big (and, thus, to avoid overflows in fixed-point DSPs).

The transfer function of the PLL can be written as [18]:

$$H_{PLL}(s) = \frac{K_p \cdot s + \frac{K_p}{T_i}}{s^2 + K_p \cdot s + \frac{K_p}{T_i}} \tag{4.1}$$

An analogy can be made with a standard second order transfer function that has a zero:

$$G(s) = \frac{2\omega_n\zeta \cdot s + \omega_n^2}{s^2 + 2\omega_n\zeta \cdot s + \omega_n^2} \tag{4.2}$$

The gains of the PI controller can be calculated as functions of the damping factor, ζ and the settling time, T_{set}:

$$K_p = \frac{9.2}{T_{set}} \tag{4.3}$$

$$T_i = \frac{T_{set}\zeta^2}{4.3} \tag{4.4}$$

where ω_n is the undamped natural frequency and $\omega_n = \frac{4.6}{\zeta T_{set}}$ [18].

Selecting a damping factor $\zeta = 0.707$ (which provides an overshoot of less than 5% in case of a step response), and a settling time $T_{set} = 0.04$, the value of the PI gains can be calculated. The obtained values are: $K_p = 230$ and $T_i = 0.0046$ (or $K_i = 50000$)

The grid phase angle obtained with the described PLL algorithm is the one presented in Fig. 4.3.

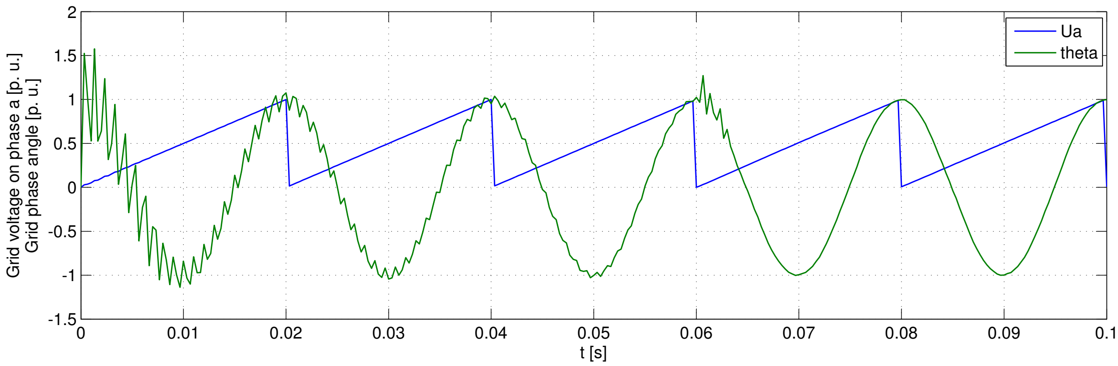

Figure 4.3: *Phase angle of the grid voltage and the grid voltage on phase a.*

4.2 Current Control

In this project, two types of current controllers are implemented: a PI control in the synchronous reference frame and a P+Resonant (PR) control in the stationary reference frame. The PI current control block diagram is given in Fig. 4.4, and the PR current control with harmonic compensation block diagram in shown in Fig. 4.5

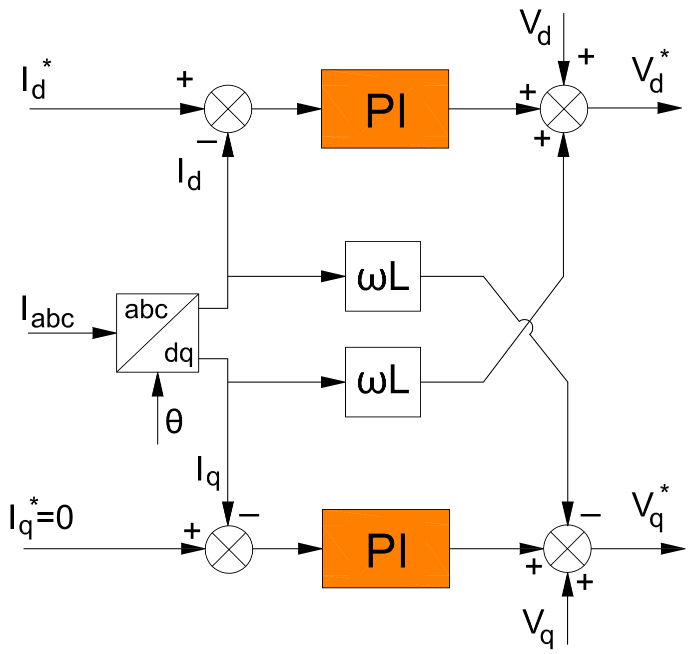

Figure 4.4: *Block diagram of the inverter PI control.*

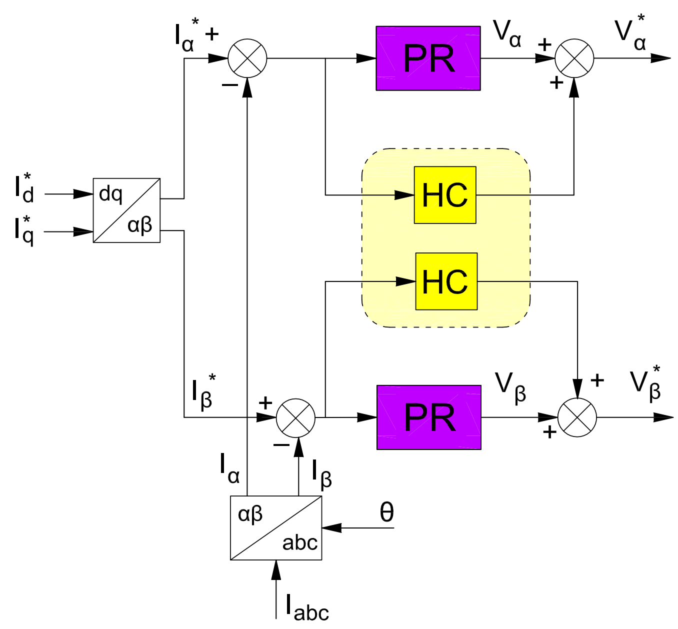

Figure 4.5: *Block diagram of the inverter PR control + Harmonic Compensation.*

At first, the controllers are tunned with an analytical method in order to obtain the values with which the discrete analysis starts. Therefore, the current controllers are firstly tuned using the optimal modulus criterion [20].

4.2.1 PI Current Control

The block diagram of the PI regulator is depicted in Fig. 4.6 and the transfer function is the one in (4.6)

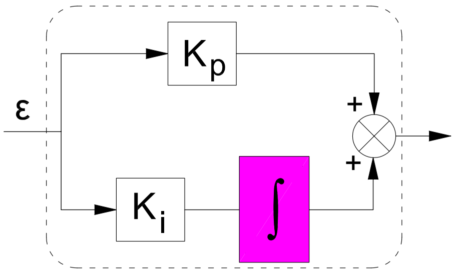

Figure 4.6: *Block diagram of PI regulator.*

$$G_{PI}(s) = K_p + \frac{K_i}{s} \tag{4.5}$$

The d and q control loops have the same dynamics, so the tuning of the PI parameters for the current control is done only for the d axis. For the q axis the parameters are assumed to be the same.

As it can be seen from the current control block diagram in Fig. 4.7, the voltage feed forward and the decoupling between the d and q axes has been neglected as they are considered as disturbances.

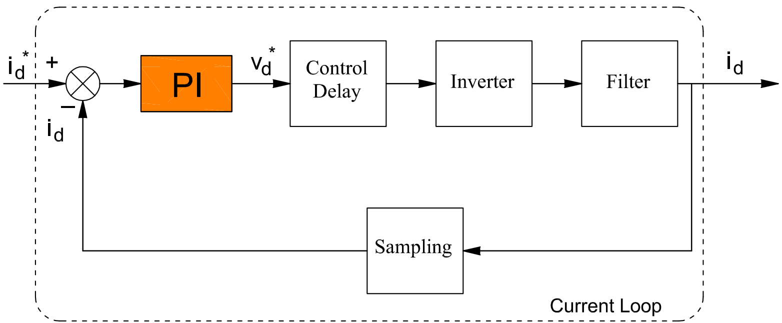

Figure 4.7: *Block diagram of the current control loop.*

This diagram can be restructured as the one in Fig. 4.8.

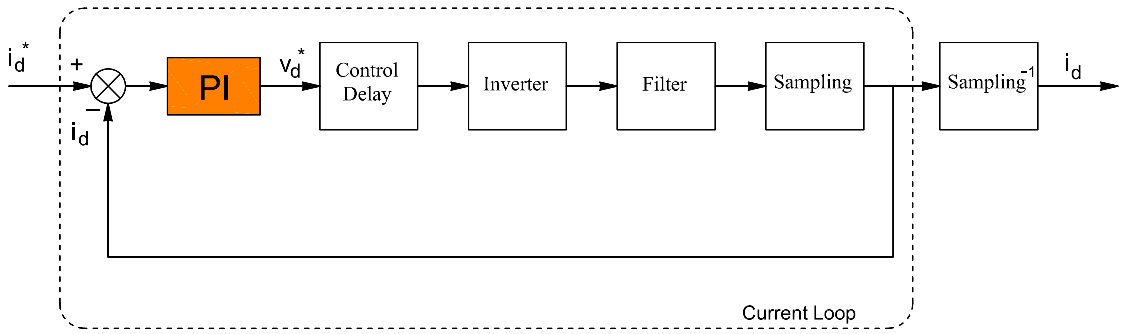

Figure 4.8: *Block diagram of the current control loop - restructured.*

In this block diagram, the following blocks are included:

- *PI* controller block with the transfer function:

$$G_{PI_{crt}}(s) = K_{p_{crt}} + \frac{K_{i_{crt}}}{s} \tag{4.6}$$

- *Control Algorithm* block with the transfer function:

$$G_{control}(s) = \frac{1}{1 + sT_s} \tag{4.7}$$

where $T_s = 1/f_s$ and $f_s = 3kHz$ is the sampling frequency.

- *Inverter* block with the transfer function:

$$G_{inverter}(s) = \frac{1}{1 + s \cdot 0.5T_{sw}} \tag{4.8}$$

where $T_{sw} = 1/(f_{sw})$ and $f_{sw} = 3kHz$ is the switching frequency of the inverter.

- *Filter* block is a simplified transfer function of the filter, that keeps into account only the the values of inductances and parasitic resistances:

$$G_{filter}(s) = \frac{1}{Ls + R} \tag{4.9}$$

where $L = L_i + L_g$ and $R = R_i + R_g$

- *Sampling* block with the transfer function:

$$G_{sampling} = \frac{1}{1 + s \cdot 0.5T_s} \tag{4.10}$$

The transfer function of the current loop can be calculated as:

$$G_{crt} = G_{PI_{crt}} \cdot G_{control} \cdot G_{inverter} \cdot G_{filter} \cdot G_{sampling} \tag{4.11}$$

Using (4.6), (4.7), (4.8), (4.9) and (4.10), the transfer function of the current loop can be written in a simplified manner as:

$$G_{crt} = \frac{K_{p_{crt}} s + K_{i_{crt}}}{s} \frac{1}{1 + sT_{\sum 1}} \frac{K_e}{sT_e + 1} \tag{4.12}$$

where $K_e = 1/R$, $T_e = L/R$ and $T_{\sum 1} = T_s + 0.5T_{sw} + 0.5T_s$

Using the optimal modulus criterion [20], the following relation can be written:

$$\frac{K_{p_{crt}} s + K_{i_{crt}}}{s} \frac{1}{1 + sT_{\sum 1}} \frac{K_e}{sT_e + 1} = \frac{1}{2sT_{\sum 1}(1 + sT_{\sum 1})} \tag{4.13}$$

From (4.13) $K_{p_{crt}}$ and $K_{i_{crt}}$ can be identified and their values calculated, as:

$$K_{p_{crt}} = \frac{T_e}{2K_e T_{\sum 1}} = 0.5 \tag{4.14}$$

$$K_{i_{crt}} = \frac{K_{p_{crt}}}{T_e} = 2.15 \tag{4.15}$$

These values are used to start the discrete analysis (using the pole placement method) using the Matlab toolbox, Sisotool. The requirements imposed on the current controller are:

- the current loop should be stable, with a phase margin larger than $45°$ and a gain margin larger than $6dB$.
- the bandwidth of the system should be minimum 500 Hz.

Using the root locus method, the proportional gain K_p is selected so that the dominant poles have a damping factor higher 0.7. As shown in Fig. 4.9, with a K_p value of 0.67, the damping of the resonant poles reaches the value of 0.9. The integral gain has been chosen as a tradeoff between a good noise rejection and good dynamics.

The zero-pole map and the Bode plot of the open-loop current control depicted in Fig. 4.9

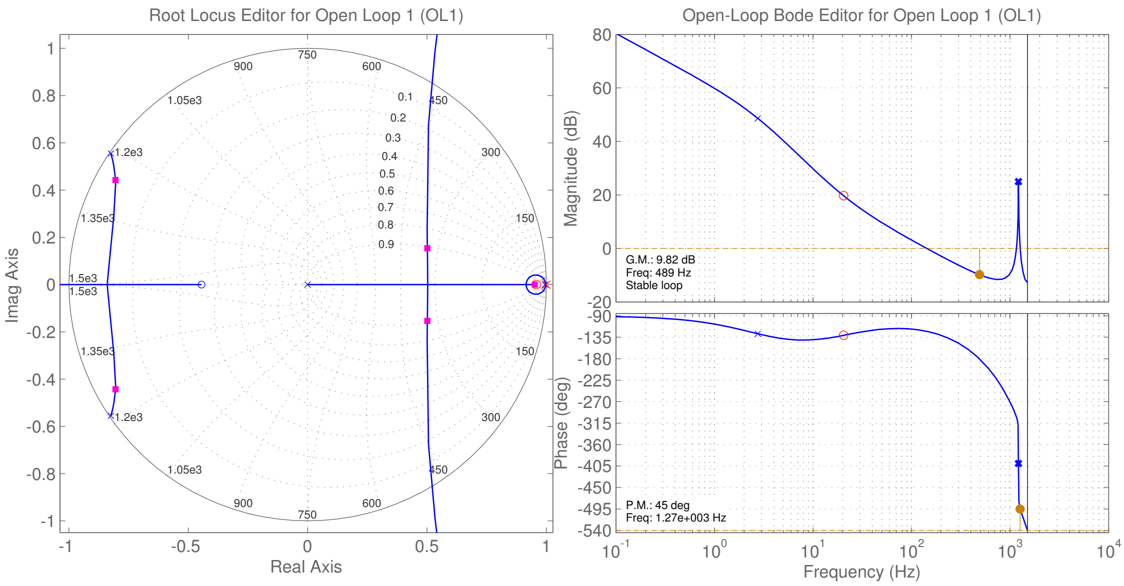

Figure 4.9: *Zero-pole map and open-loop Bode plot of the PI current control.*

Fig. 4.9 also shows that the control has a phase margin of $45°$ and a gain margin of $9.82dB$.

The step response is plotted in Fig. 4.10. It can be seen that a settling time of 0.01 is obtained.

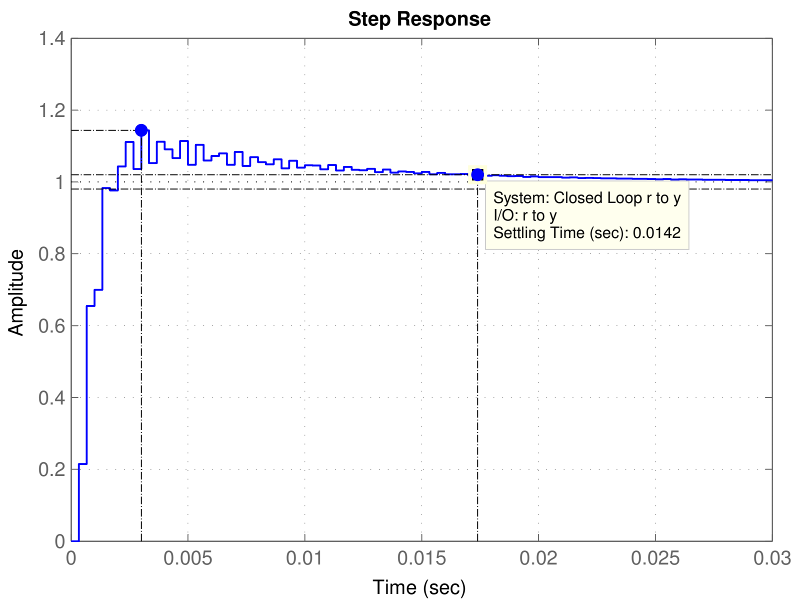

Figure 4.10: *Step response of the PI current control loop.*

4.2.2 PR Current Control

The block diagram of the PR regulator with Harmonic Compensation is depicted in Fig. 4.11 .

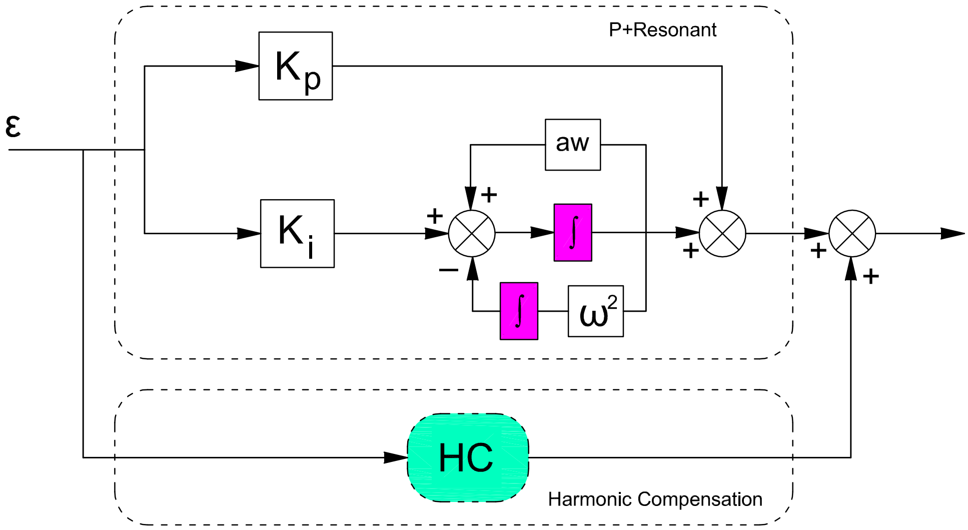

Figure 4.11: *Block diagram of PR regulator.*

The transfer function of the PR controller is [21]:

$$G_{PI}(s) = K_p + K_i \frac{s}{s^2 + \omega^2} \tag{4.16}$$

where aw is the anti-windup function implemented as:

$$aw = \begin{cases} y_{max} - y, & y > y_{max} \\ \\ y - y_{max}, & y < -y_{max} \end{cases} \tag{4.17}$$

The transfer function of the Harmonic Compensator is[21]:

$$G_{HC}(s) = \sum K_{Ih} \frac{s}{s^2 + (\omega \cdot h)^2}, h = 3, 5, 7 \tag{4.18}$$

The most important harmonics in the current spectrum are the 3rd, the 5th and the 7th. So the harmonic compensator is designed to compensate these three selected harmonics.

In order to perform the discrete analysis on the PR current control, the initial values calculated with the optimal modulus method for the PI control are used for the PR control to begin with.

Using the root locus method, the proportional gain K_p is selected so that the dominant poles have a damping factor of 0.7. As it can be seen in the Fig. 4.12, with a K_p value of 0.78, the damping of the resonant poles reaches the value of 0.7. An integral gain K_i of 300 has been chosen as a tradeoff between a good noise rejection and good dynamics.

The zero-pole map and the Bode plot of the open-loop current control depicted in Fig. 4.12

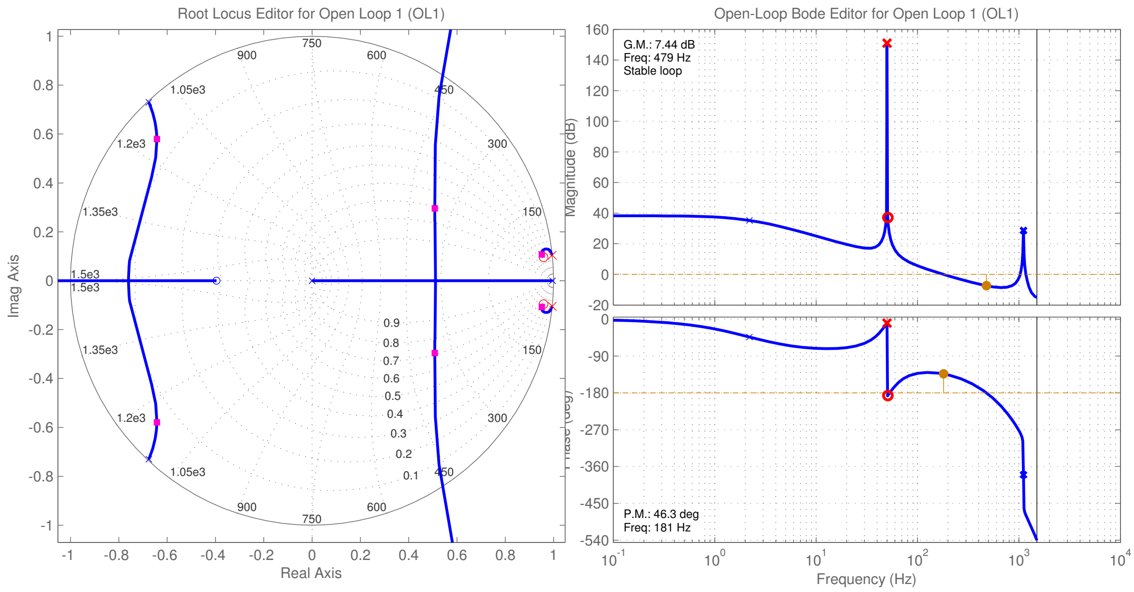

Figure 4.12: *Zero-pole map and open-loop Bode plot of the PR current control.*

Fig. 4.12 also shows that the control has a phase margin of $46.3°$ and a gain margin of $7.44dB$.

The Bode plot of closed-loop current control is plotted in Fig. 4.13. It shows that the bandwidth of the current controller has a value of approximately 500Hz.

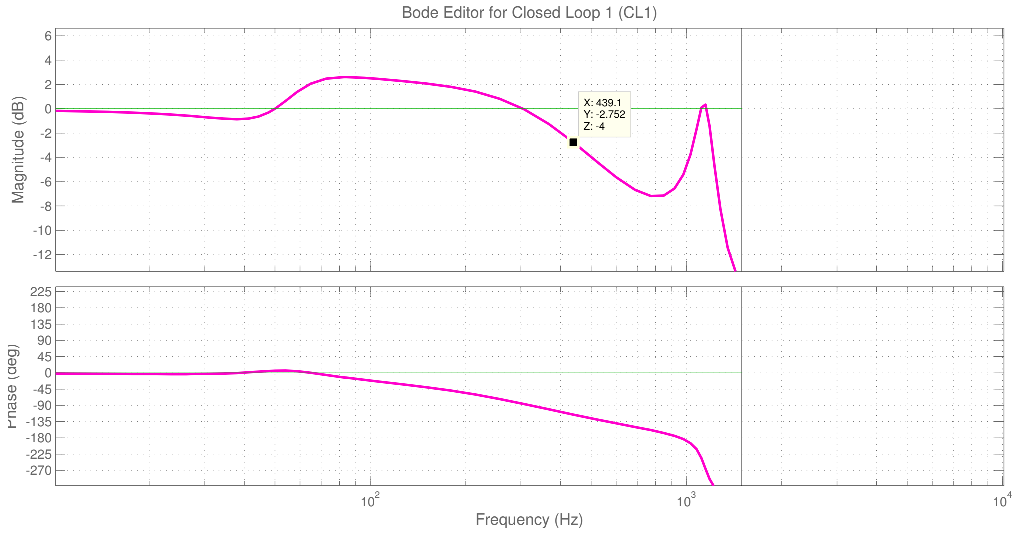

Figure 4.13: *Closed-loop Bode plot of the PR current control.*

The step response is plotted in Fig. 4.14. It can be seen that a settling time of 0.02 is obtained.

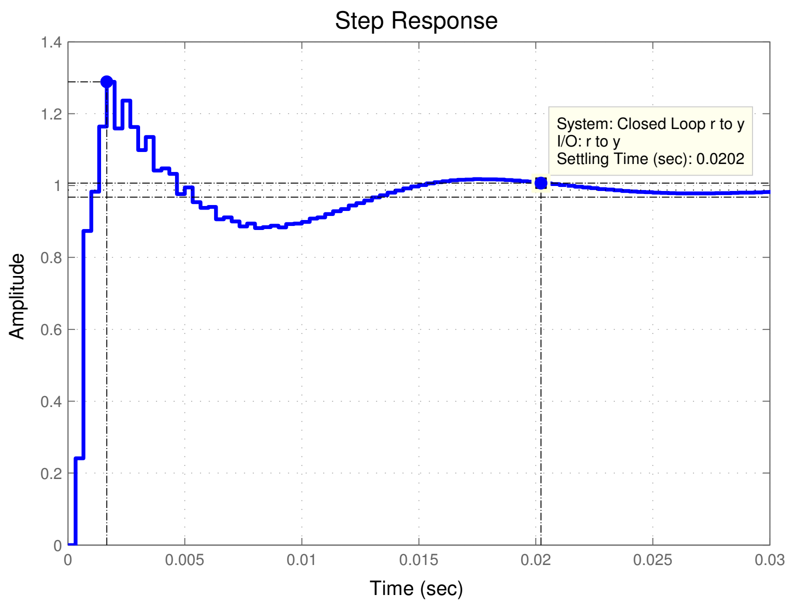

Figure 4.14: *Step response of the PR current control loop.*

4.3 DC Voltage Control

As in the case of the dc voltage loop, the controllers are tunned with an analytical method in order to obtain the values with which the discrete analysis starts. Thus, the dc voltage controller is tuned using the optimum symmetrical criterion [22].

The closed loop transfer function of the current loop can be written as:

$$G_{crt_{closed}} = \frac{1}{2sT_{\sum 1}(1 + sT_{\sum 1}) + 1} \approx \frac{0.5sT_s + 1}{2sT_{\sum 1} + 1} \tag{4.19}$$

The dc voltage control block diagram is shown in Fig. 4.15.

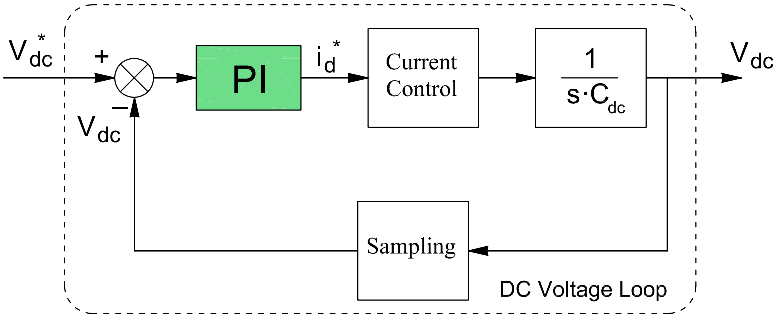

Figure 4.15: *Block diagram of the voltage dc control loop.*

This diagram can be restructured as the one in Fig. 4.16.

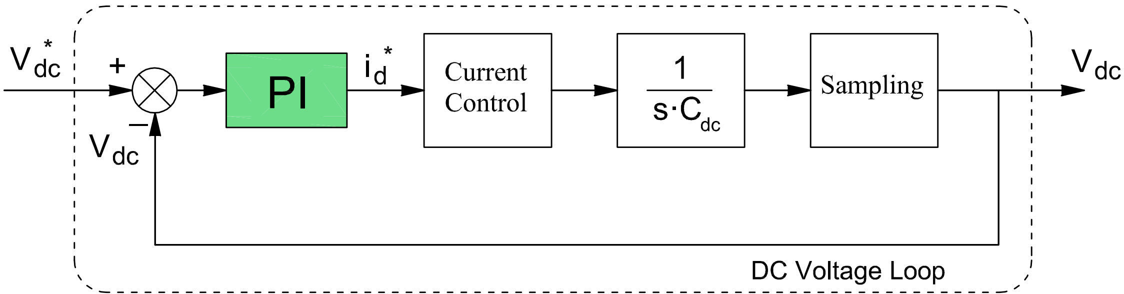

Figure 4.16: *Block diagram of the dc voltage loop - restructured.*

The values of the PI controller are calculated using the method called optimum symmetrical [22]. Firstly, a phase margin ψ of $45°$ is imposed.

Considering

$$a = \frac{1 + cos\psi}{sin\psi} \tag{4.20}$$

the PI parameters can be calculated as:

$$K_{p_{vol}} = \frac{4C_{dc}}{2T^2_{\sum 2}9aT_s} = 2.77 \tag{4.21}$$

$$K_{i_{vol}} = \frac{K_{p_{vol}}}{3 \cdot a^2 \cdot T_s} = 482.2 \tag{4.22}$$

Using the pole placement method, a discrete analysis has been performed with the Matlab toolbox, Sisotool.

With a proportional gain $K_p = 1.7$ a stable loop with a phase margin of $59.1°$ and a gain margin of $18.5dB$ are obtained, as shown in Fig. 4.17.

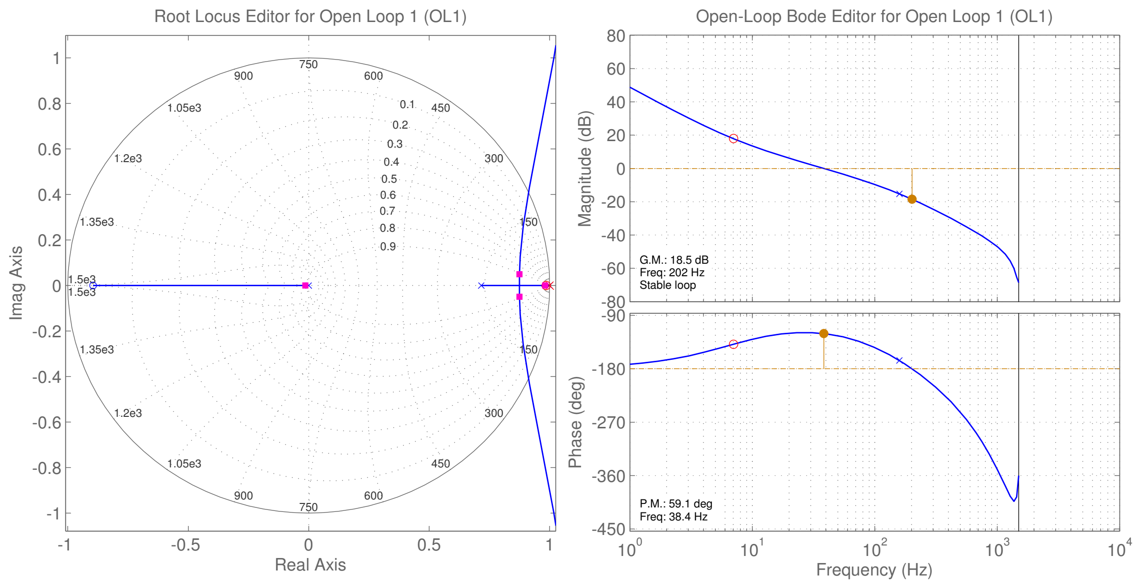

Figure 4.17: *Zero-pole map and Bode plots of the voltage control loop.*

The settling time for the voltage loop is 0.05s. The step response is plotted in Fig. 4.18.

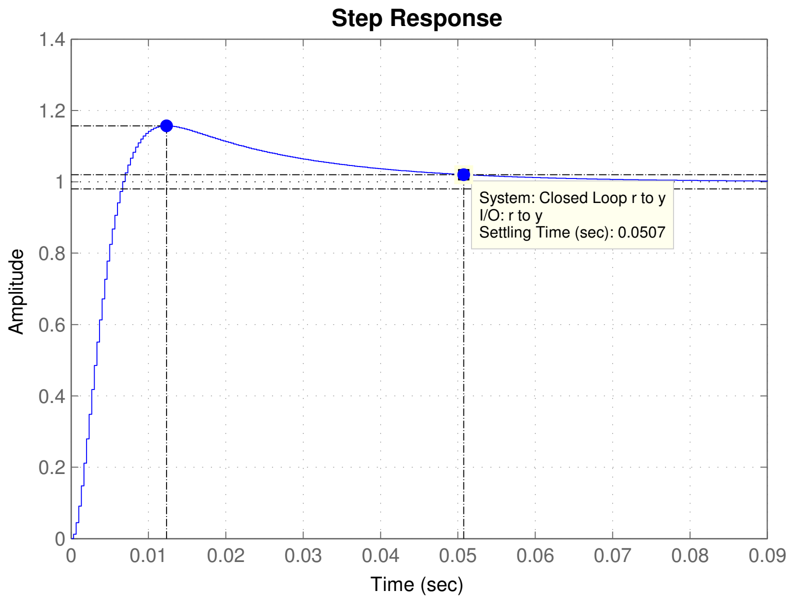

Figure 4.18: *Step response of the voltage control loop.*

Active Damping

5

This chapter deals with the implementation of two active damping methods: notch filter and virtual resistor. For each of them, the frequency response is studied, as well as the effect of the changes in the grid values and in the filter parameters.

5.1 Notch Filter

5.1.1 Transfer function and frequency response

As stated before in section 2.3.3, a method to obtain active damping is to introduce in the current loop a notch filter, tuned at the resonance frequency of the LCL filter.

The transfer function of the notch filter is:

$$H_{notch}(s) = \frac{s^2 + 2\zeta_2\omega_0 s + \omega_0^2}{s^2 + 2\zeta_1\omega_0 s + \omega_0^2} \tag{5.1}$$

The dependence between ζ_1 and ζ_2 can be expressed by: [12]

$$\begin{cases} \zeta_2 < \zeta_1 \\ \zeta_2 = \zeta_1/\alpha \end{cases} \tag{5.2}$$

The term α is related to the resistance of the grid (R_{grid}) and can be expressed as:

α = $k\cdot$ R_{grid} (k is a constant). ω_0 is the cutooff frequency of the notch filter and is related to the resonance frequency of the LCL filter.

Considering the LCL filter designed before, in section 3.5, with the transfer function stated in (3.10) and the transfer function of the notch filter stated in (5.1), the frequency response of the system can be analised, from the Bode plot depicted in Fig. 5.1.

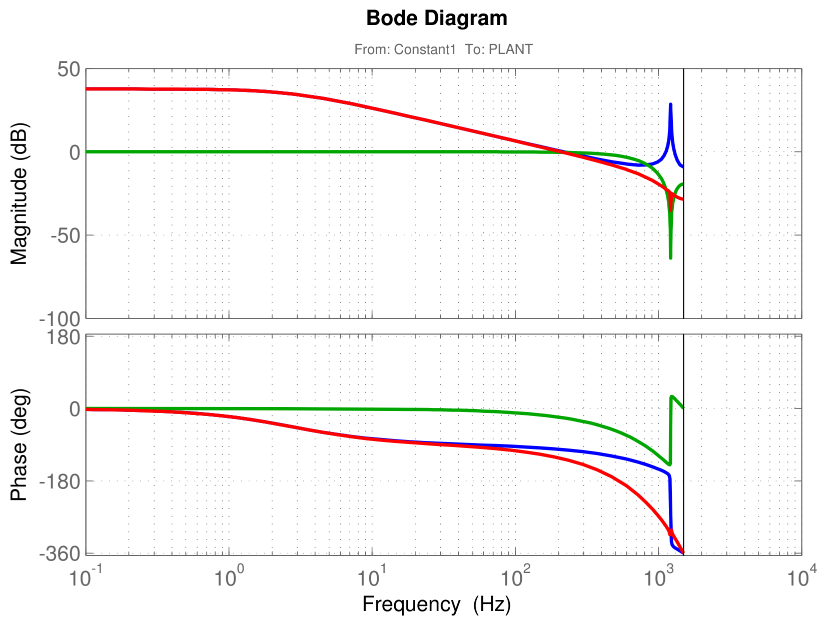

Figure 5.1: *Bode Plot of LCL filter, notch filter and the two in series.*

The notch filter introduces in the system two zeros and two poles. The root loci and the open loop bode plots without and with the notch filter are shown in Fig. 5.2 and Fig. 5.3

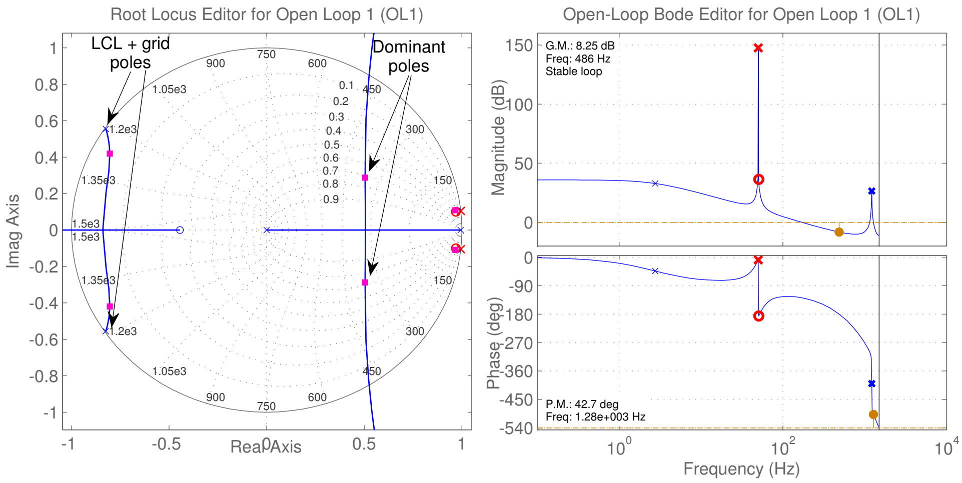

Figure 5.2: *Root loci and open-loop Bode diagram of the current loop without notch filter.*

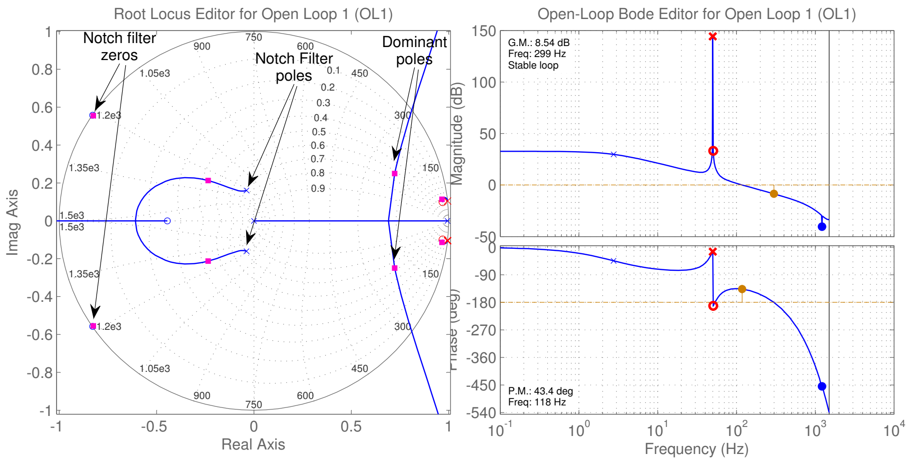

Figure 5.3: *Root loci and open-loop Bode diagram of the current loop with notch filter.*

5.1.2 Effect of changes in grid inductance

The fluctuations of the grid inductance affects the resonance frequency, as the resonance frequency of the filter, considering the grid inductance (L_{grid}), is calculated as:

$$\omega_{res} = \sqrt{\frac{L_i + (L_g + L_{grid})}{L_i \cdot (L_g + L_{grid}) \cdot C_f}} \tag{5.3}$$

An increase in the grid inductance leads to a decrease in the resonance frequency and a decrease in the grid impedance leads to an increase in the resonance frequency. This means that some kind of grid condition detection algorithm should be used, in order to accurately tune the notch filter.

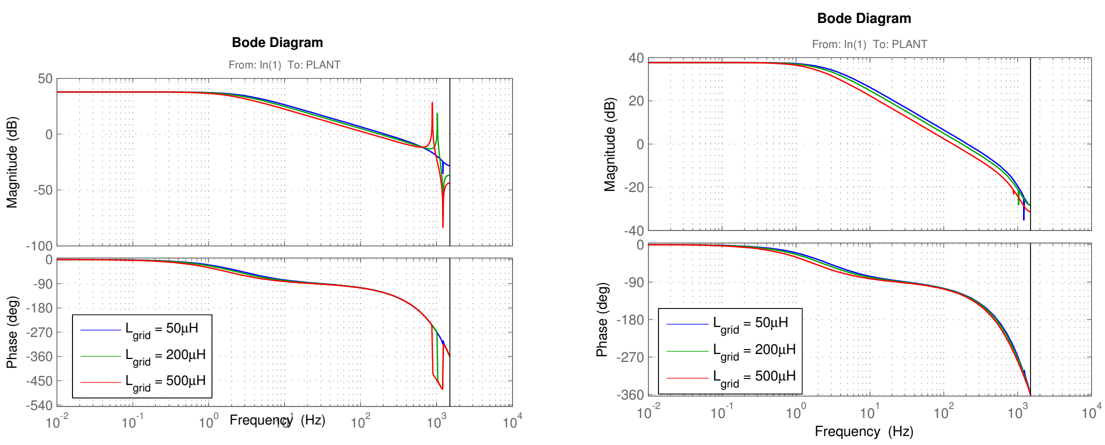

(a) Grid detection is not used. (b) Grid detection is used.

Figure 5.4: *Bode Plots of LCL filter plus grid inductance and notch filter at grid fluctuations.*

In Fig. 5.4 (a) is shown the frequency response of the LCL filter plus grid impedance and notch filter, when no grid detection algorithm is used, but just an assumption that the grid inductance is $L_{grid} = 50\mu H$. It can be seen that if the grid inductance is a lot different from the assumption, the notch filter is no longer efficient, as it is tuned on a frequency which is not the resonance frequency. However, if a grid detection method is used (as it is the case in Fig. 5.4) (b), then the notch filter effectively damps the resonance frequency.

5.1.3 Effect of changes in the values of LCL filter components

Sometimes, during extensive use, the filter components can sustain changes in their values, due to high temperatures or ageing. Fig. 5.5 (a) and (b) show how the frequency response of the LCL filter plus grid impedance and notch filter, changes when the value of the filter capacitance and the inverter side inductance changes with $\pm 10\%$.

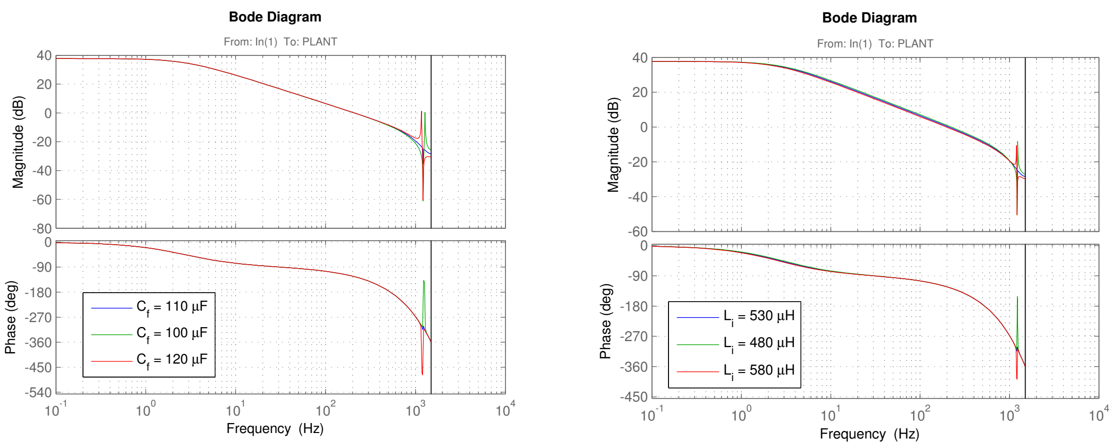

(a) C_f varies with $\pm 10\mu F$.

(b) L_i varies with $\pm 50\mu H$.

Figure 5.5: *Bode Plots of LCL filter plus grid impedance and notch filter when the LCL filter components vary.*

It can be seen that the change in the capacitance value produces a loss in the efficiency of the notch filter, though not making its presence completely useless, as a certain amount of damping still exists. The change in the inductance value has even smaller effects on the efficiency of the notch filter, because the resonance frequency is not modified much.

5.2 Virtual Resistance

5.2.1 Frequency response

As stated before, the idea of the virtual resistance method is to simulate the behavior of passive damping, without actually using a damping resistance in the setup. Out of the four positions the damping resistance can be placed in, two are investigated in this project: in series with the filter capacitance and in series with the inverter side inductance.

Fig. 5.6.a and Fig. 5.6.b show how the frequency response of the filter is modified when a virtual damping resistance with different values is used, in the two positions mentioned before.

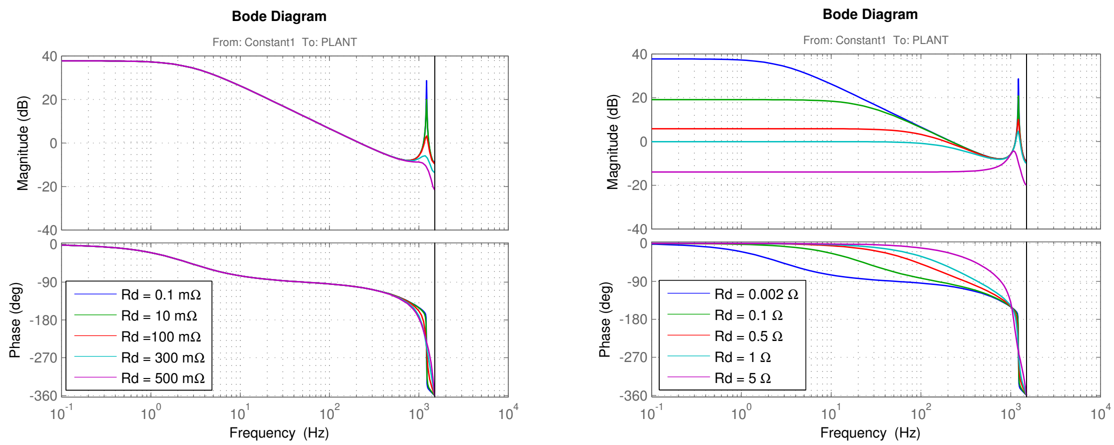

(a) R_d in series with the filter capacitance. (b) R_d in series with the filter inductance.

Figure 5.6: *Bode Plots of LCL filter with different damping resistances.*

When the virtual damping resistance is connected in series with the filter capacitance, the attenuation around the switching frequency, gets lower as the resistance is increased. When the damping resistance is connected in series with the inverter side inductance, the attenuation remains the same around the switching frequency, but the resonance frequency is decreased as the resistance is increased.

The root loci plots show that the effect of virtual damping resistance in the control loop attracts the resonant poles of the filter towards the inside of the circle, providing a considerable amount of damping. The root loci and the open loop bode plots of the system with virtual damping resistance connected in series with the filter capacitance and with the inverter side inductance are shown in Fig. 5.7 and Fig. 5.8

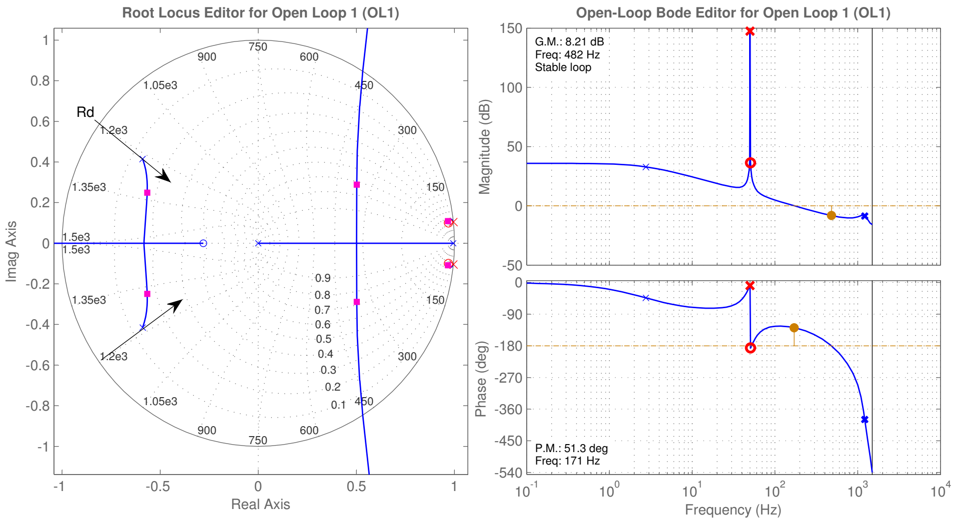

Figure 5.7: *Root loci and open-loop Bode diagram of the current loop with virtual damping resistance in series with C_f.*

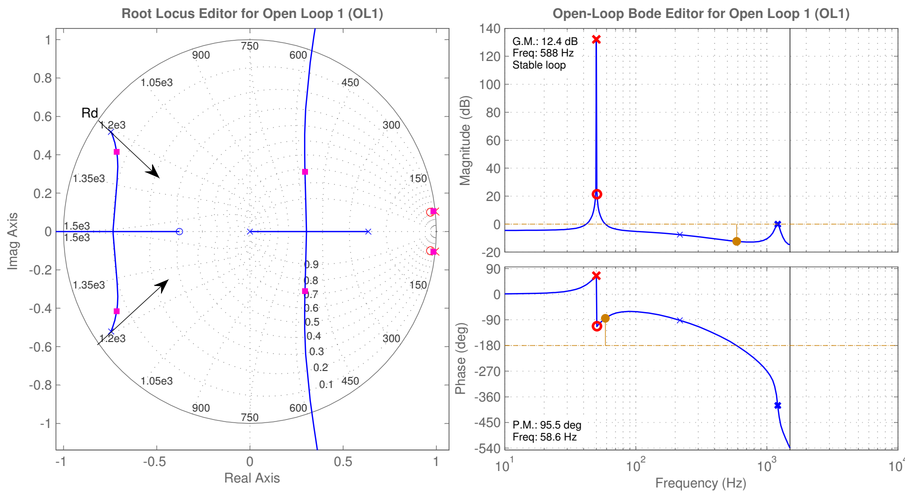

Figure 5.8: *Root loci and open-loop Bode diagram of the current loop with virtual damping resistance in series with L_i.*

5.2.2 Effect of changes in the grid inductance

Like for the notch filter method, the effect of the changes in the grid inductance changes is studied, in the case of virtual damping resistance connected in series with the filter capacitance and with the grid side inductance.

The tests have been performed with a virtual damping resistance of $300m\Omega$ when the resistance was in series with the filter capacitance, and a virtual damping resistance of 5Ω when the resistance was in series with the grid side inductance.

Figure 5.9: *Bode Plots of LCL filter with virtual damping resistance when the grid impedance varies.*

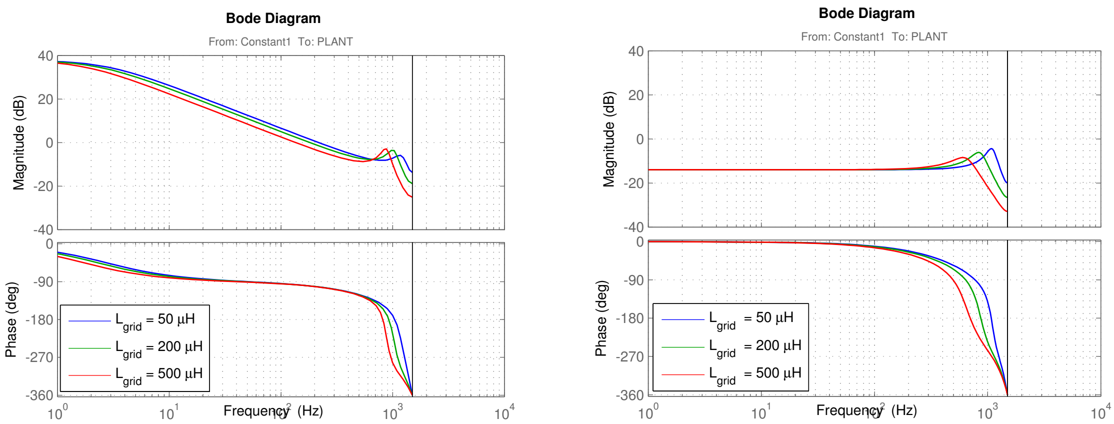

(a) R_d in series with the filter capacitance.

(b) R_d in series with the inverter side inductance.

As it can be seen in Fig. 5.9 (a) and (b), the variation of the grid inductance affects just a little the damping of the resonance frequency, but the system is still very well damped.

5.2.3 Effect of changes in the values of LCL filter components

As in the case of active damping with notch filter, a study has been made in the case of the virtual resistance method, to investigate how the frequency response of the system changes when the components of the LCL filter experience changes in their values.

Fig. 5.10.a and Fig. 5.10.b show how the frequency response of the LCL filter with a virtual damping resistance connected in series with the filter capacitance, changes when the value of the filter capacitance and the inverter side inductance changes with $\pm 10\%$.

Fig. 5.11.a and Fig. 5.11.b show how the frequency response of the LCL filter with a virtual damping resistance connected in series with the filter capacitance, changes when the value of the filter capacitance and the inverter side inductance changes with $\pm 10\%$.

Figure 5.10: *Bode Plots of LCL filter with virtual damping resistance connected in series with the filter capacitance when the LCL filter components vary.*

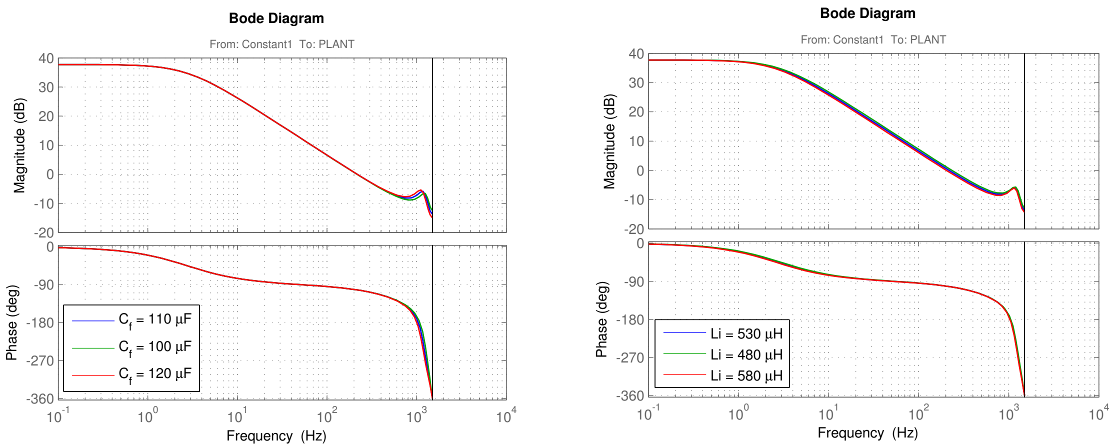

(a) C_f varies with $\pm 10\mu F$.

(b) L_i varies with $\pm 50\mu H$.

Figure 5.11: *Bode Plots of LCL filter with virtual damping resistance connected in series with the filter inductance when the LCL filter components vary.*

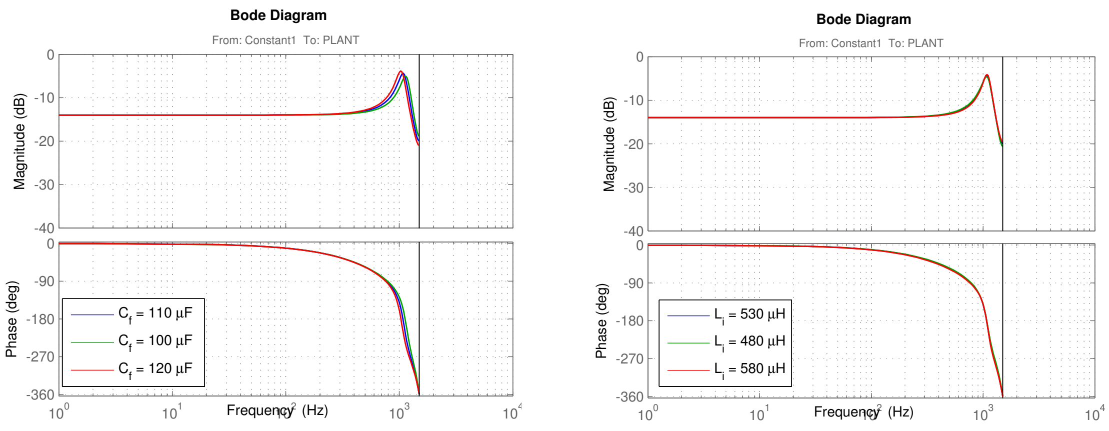

(a) C_f varies with $\pm 10\mu F$.

(b) L_i varies with $\pm 50\mu H$.

The frequency responses show that, both in the case of virtual damping resistance connected in series with the filter capacitance and in the case of virtual damping resistance connected in series with the inverter side inductance, the damping of the system is robust, by being quite insensitive to the changes in the values of the filter parameters.

Simulation results 6

This chapter contains the different simulation results that have been obtained using Matlab/Simulink. It in structured into two sections: the first one contains simulation results that confirm the good design of the PI and PR current controllers and of the dc voltage controller. The second one contains simulation results that confirm that active damping has been achieved on the resonance frequency of the LCL filter.

6.1 Simulation of a grid connected system using LCL filter

There have been chosen two simulation cases that confirm the good design of the controllers.

6.1.1 Case 1: Steps in the active power on the system with PI current control

The reference for the active power has been varied in five steps, each with the width of 100ms. The first step is at 0.8 of the rated power, the next is at the rated power, then 0.8 again, then 0.6 of the rated power and the last is back at 0.8. The reference and the measured active power are plotted in Fig. 6.1. It can be noticed that the measured power tracks the reference very well .

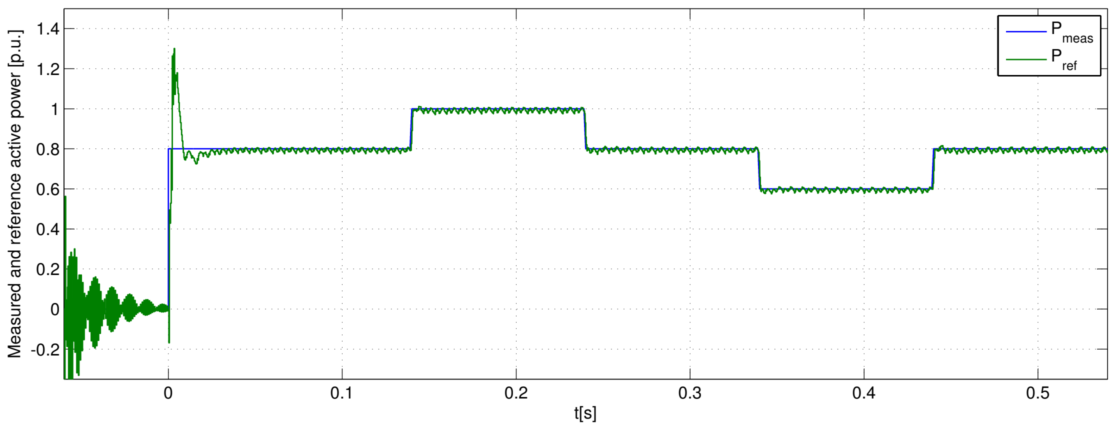

Figure 6.1: *Reference and measured active power in the simulation Case 1.*

The reactive power reference has been set to 0. The reference and the measured reactive power are plotted in Fig. 6.2.

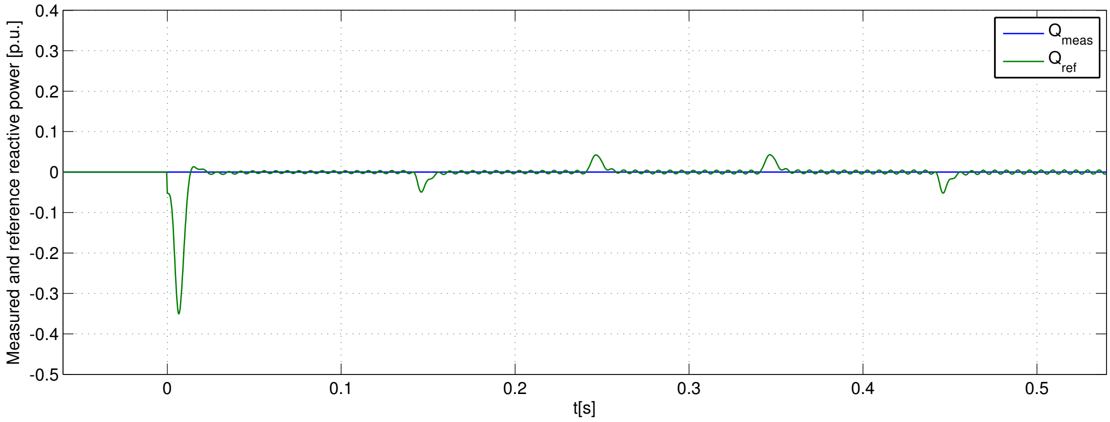

Figure 6.2: *Reference and measured reactive power in the simulation Case 1.*

The d and q components of the measured grid currents are plotted in Fig. 6.3. As i_d determines the active power, it can be seen that its reference changes proportionally with the active power, while i_q is kept at a 0 reference, given by the reactive power.

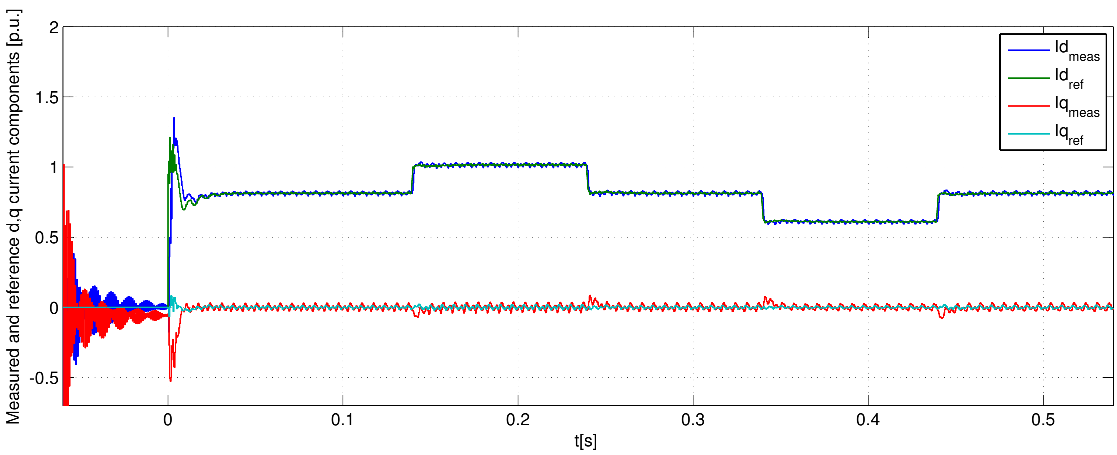

Figure 6.3: *Reference and measured d and q current components in the simulation Case 1.*

Fig. 6.4 shows the measured grid currents, as well as a zoom at the point of a step in the power reference.

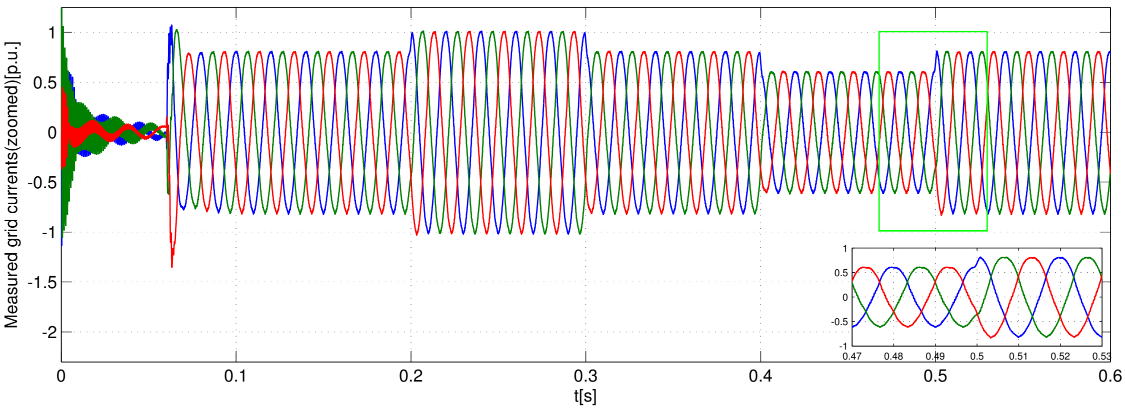

Figure 6.4: *Measured grid currents in the simulation Case 1.*

The measured dc voltage is plotted in Fig. 6.5. This plot shows that the dc voltage is kept at a constant level (1 p.u.) in the case of a power variation.

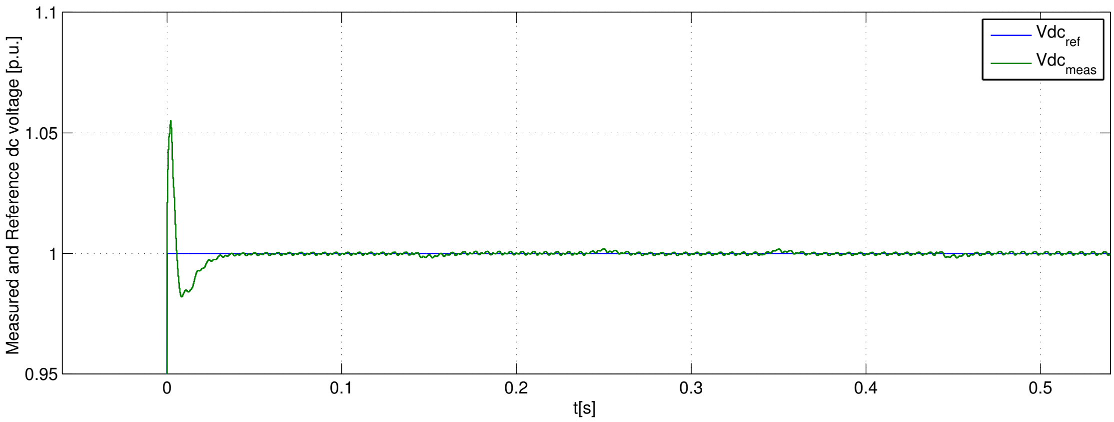

Figure 6.5: *Measured dc voltage in the simulation Case 1.*

6.1.2 Case 2: Steps in the active power on the system with PR current control

As in the simulation Case 1, the reference for the active power has been varied in five steps, each with the width of 100ms. The first step is at 0.8 of the rated power, the next is at the rated power, then 0.8 again, then 0.6 of the rated power and the last is back at 0.8. The reference and the measured active power are plotted in Fig. 6.6.

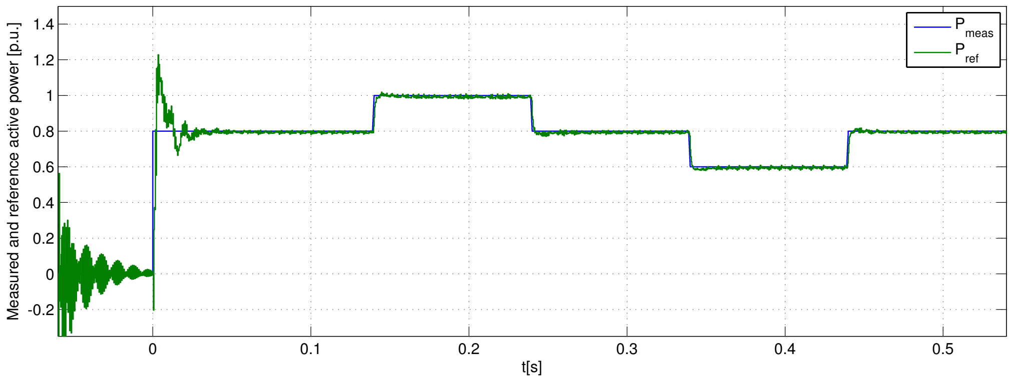

Figure 6.6: *Reference and measured active power in the simulation Case 2.*

The reactive power reference has been set to 0. The reference and the measured reactive power are plotted in Fig. 6.7.

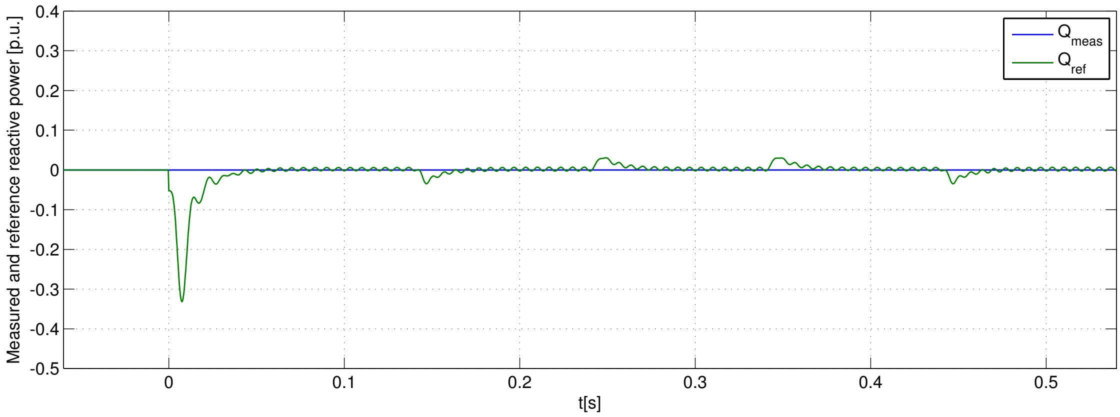

Figure 6.7: *Reference and measured reactive power in the simulation Case 2.*

Fig. 6.8 shows the measured grid currents, as well as a zoom at the point of a step in the power reference.

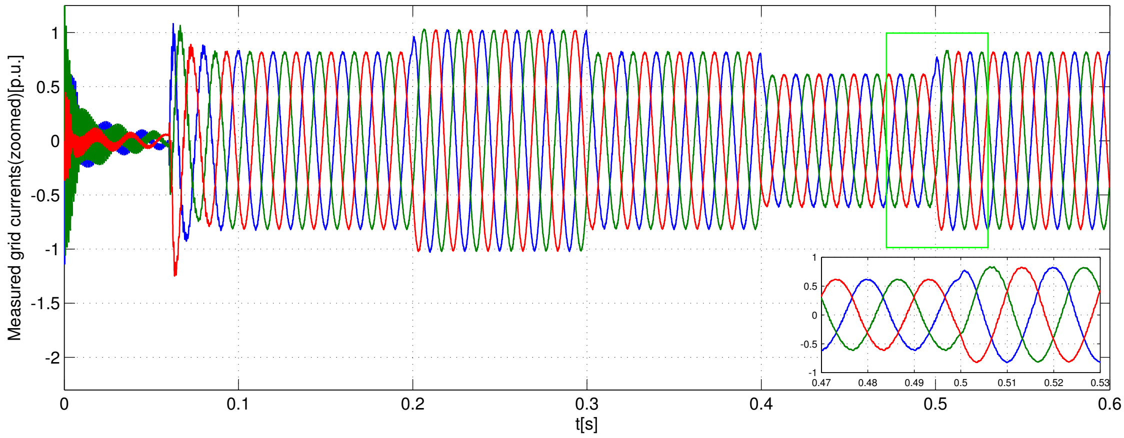

Figure 6.8: *Zoom on the measured grid currents in the simulation Case 2.*

The measured dc voltage is plotted in Fig. 6.9. This plot shows that the dc voltage is kept at a constant level (1 p.u.) in the case of a power variation.

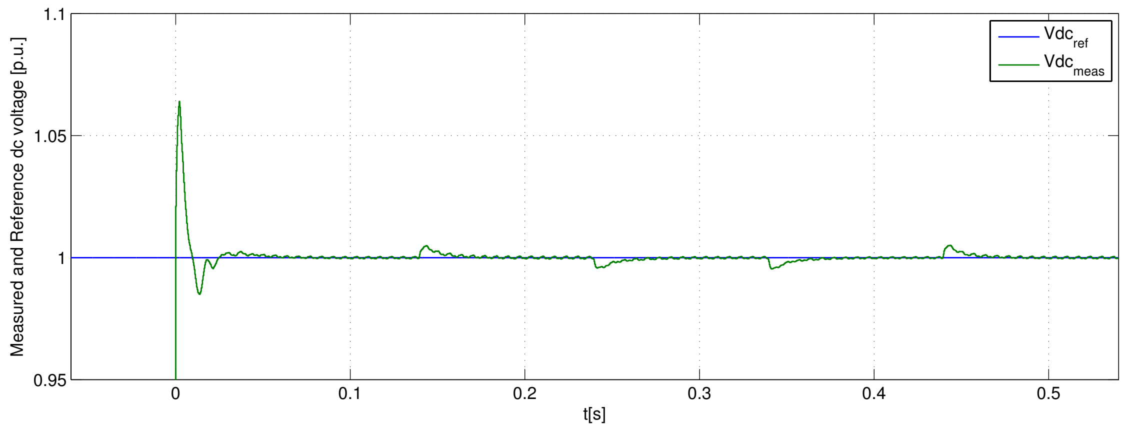

Figure 6.9: *Measured dc voltage in the simulation Case 2.*

6.2 Active Damping of the LCL filter resonance

In order to test the behavior of the system under the implemented active damping methods, two types of tests have been performed. As the P+Resonant current controller was the one that provided better performances in simulations, the tests were implemented using this controller. In the first test, the proportional gain of the controller has been increased until close to the instability limit, to a value of $K_p = 0.92$ and the system started with no damping. After $0.1s$, the active damping method has been switched on. This test is meant to show the performance and efficiency of the control. In the second test, a step in the current reference has been simulated, with two different values of the proportional gain, in order to show the improvement of the step response of the system as the proportional gain is allowed to be increased by active damping. This test is meant to show the robustness of the control.

6.2.1 Notch Filter

The proportional gain of the control has been set to $Kp = 0.92$, which is close to the stability limit for the undamped system. The Notch filter is introduced in the system at $0.1s$. The measured grid currents are shown in Fig. 6.10.

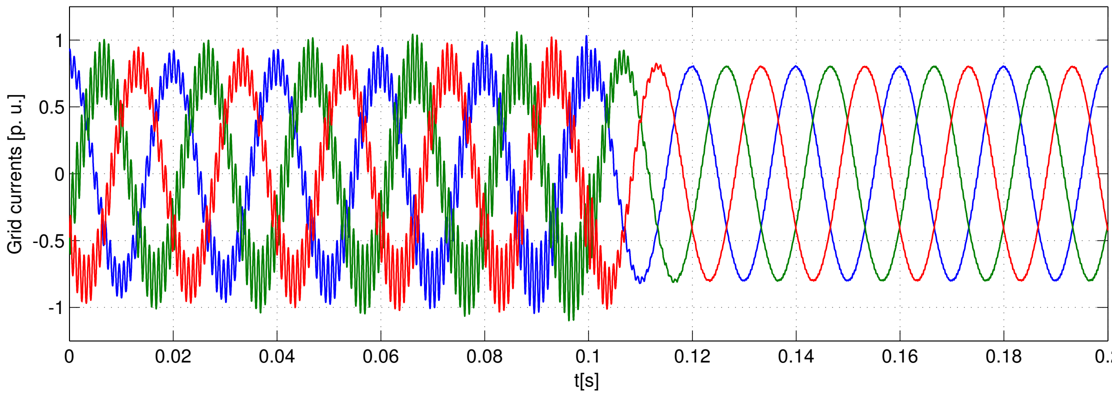

Figure 6.10: *Measured grid currents in the case of notch filter switched on at* $0.1s$.

The plot shows that the currents stabilize within one period after introducing the notch filter in the system, thus proving the efficiency of the control.

In the next test, the a step in the current reference has been simulated (from 0.8 p.u. to 1 p.u.), with two values of the proportional gain. Fig. 6.2.1 shows the system simulated with no active damping, first with a $K_p = 0.78$ (a) and then with a higher value, $K_p = 0.92$ (b).

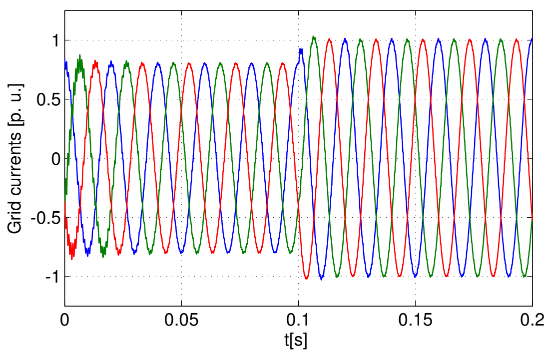

(a) Proportional gain $K_p = 0.78$.

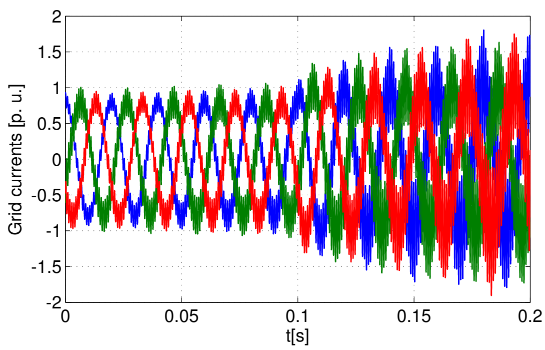

(b) Proportional gain $K_p = 0.92$.

Figure 6.11: *Step in the current reference of the undamped system*

A similar test has been performed on the system with a notch filter in the current loop. Fig. 6.12 shows the results, first with $K_p = 0.78$ (a) and then with $K_p = 2$.

Figure 6.12: *Step in the current reference of the system actively damped with a notch filter.*

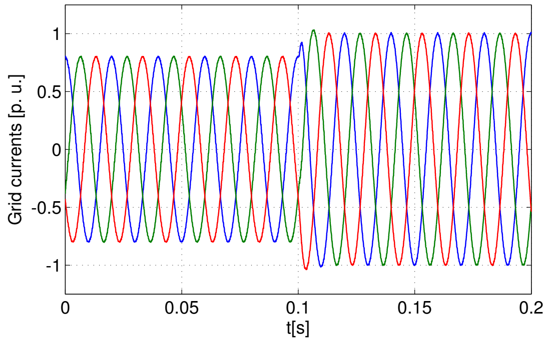

(a) Proportional gain $K_p = 0.78$.

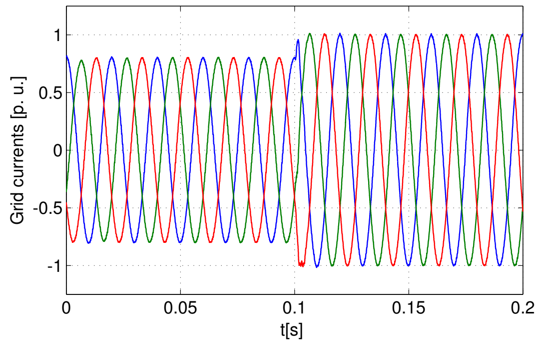

(b) Proportional gain $K_p = 2$.

It can be noticed that even with a K_p of 2, the system damped with the notch filter is stable whereas, the undamped system is unstable already at a $K_p = 0.92$. The fact that the system actively damped with the notch filter stays stable for a higher proportional gain, means that by introducing the notch filter in the system, both the performance and the robustness of the current controller are increased.

6.2.2 Virtual resistance

As in the case of active damping with notch filter, the first test performed is a switching on of the active damping method, when the system runs close to the stability limit.

Fig. 6.13 shows the measured grid currents in the case when a damping resistance of $300m\Omega$ is considered in series with the filter capacitance.

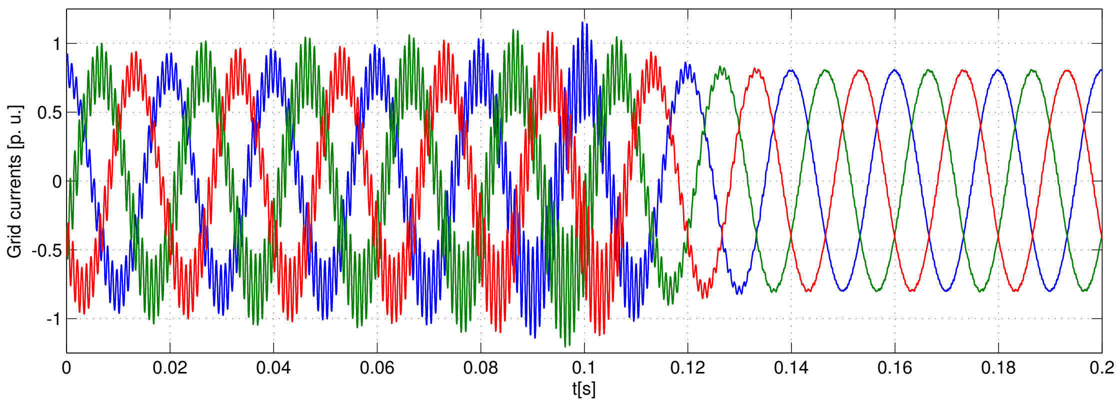

Figure 6.13: *Measured grid currents in the case of virtual resistance in series with C_f switched on at $0.1s$.*

Fig. 6.14 shows the measured grid currents in the case when a damping resistance of 2Ω is considered in series with the inverter side inductance.

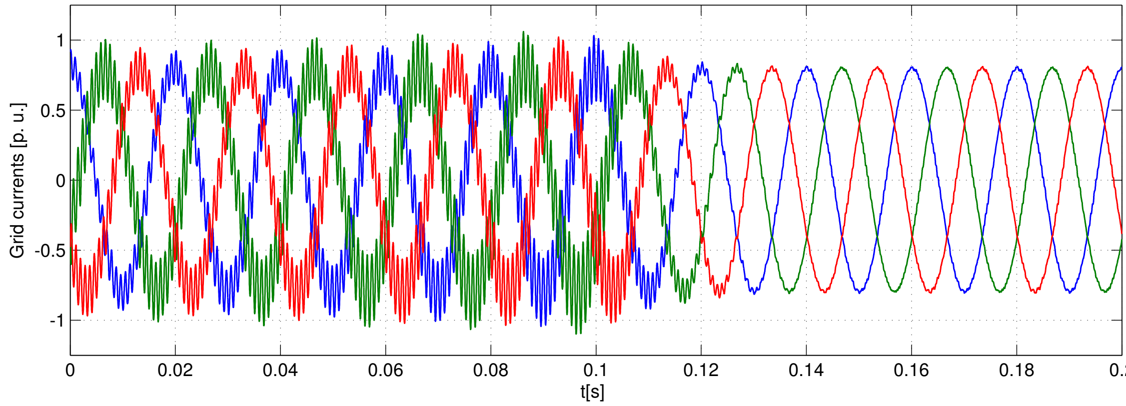

Figure 6.14: *Measured grid currents in the case of virtual resistance in series with L_i switched on at $0.1s$.*

Fig. 6.14 shows that the system passes to stability in the first period after the virtual damping resistance is introduced in the current loop.

The second test simulates again the behavior of the system in the case of a step in the current reference from $0.8p.u.$ to $1p.u.$, first with a small proportional gain, then with a bigger one.

When the virtual damping resistance is considered in series with the filter capacitance, the results obtained with a K_p of 0.78 and a K_p of 1 are shown in Fig. 6.15.

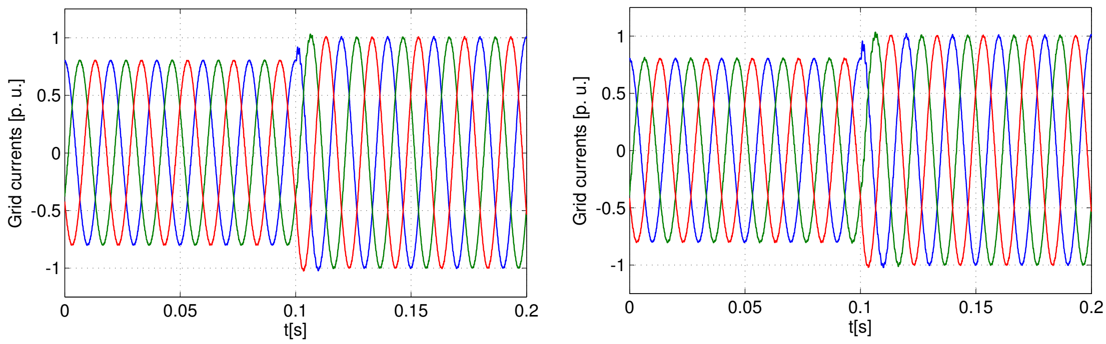

(a) Proportional gain $K_p = 0.78$. (b) Proportional gain $K_p = 1$.

Figure 6.15: *Step in the current reference of the system damped with a virtual resistance in series with C_f*

When the virtual damping resistance is considered in series with the inverter side inductance, the results obtained with a K_p of 0.78 and a K_p of 1 are shown in Fig. 6.16.

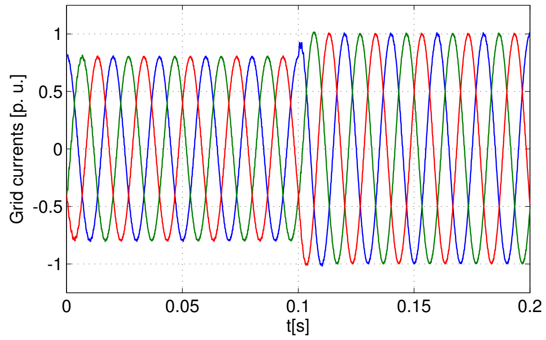

(a) Proportional gain $K_p = 0.78$.

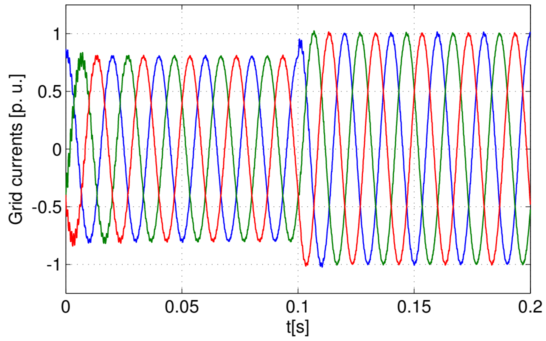

(b) Proportional gain $K_p = 1$.

Figure 6.16: *Step in the current reference of the system damped with a virtual resistance in series with L_i*

Like in the case of the notch filter method, also in the case of the virtual resistance method, the system remains stable for a larger proportional gain than in the case of an undamped system. However, it was noticed that the value of K_p can be raised less, than in the case of the notch filter, method before leading the system into instability. Even so, by using the virtual resistance damping method, the system gains robustness and performance.

7 Experimental Results

This chapter contains the description of the setup in the laboratory. Moreover, the experimental results, that confirm the simulations, are described and discussed.

7.1 Experimental setup

The system used in simulations has been downscaled to a lower power level, 2.2kVA, due to the available devices in the laboratory. The experimental setup is the one in Fig. 7.1 and its block diagram is depicted in Fig. 7.2.

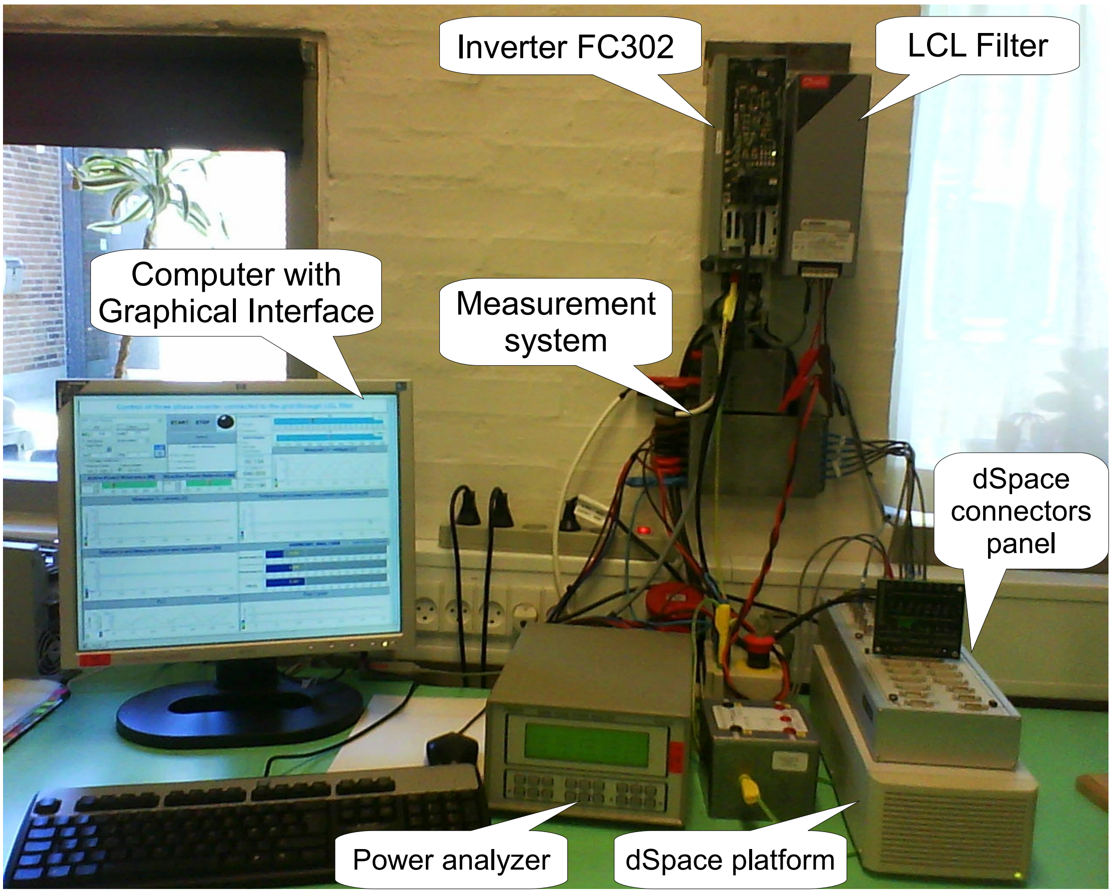

Figure 7.1: *Experimental setup.*

The LCL filter consists of an LC filter and, on the grid side, the transformer's inductance of 2mH.

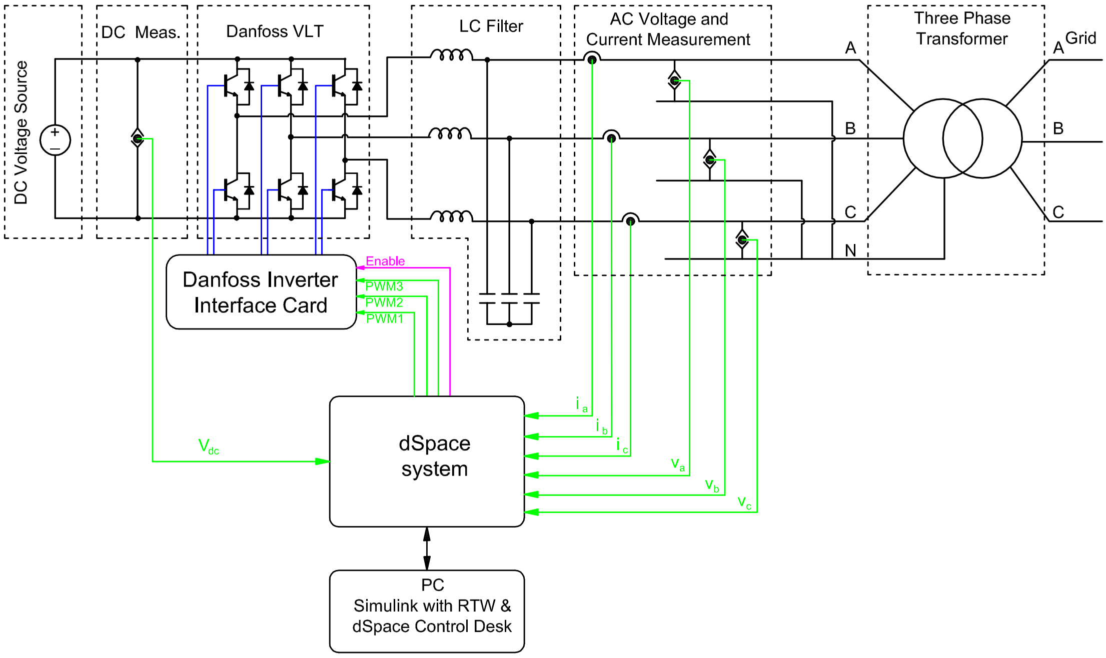

Figure 7.2: *Block diagram of the experimental setup.*

The setup consists of:

- **Dafoss Inverter FC302**
  - Rated power: *2.2kVA*
  - Rated input frequency: *50-60 Hz*
  - Rated output voltage: *3x230 V*
  - Rated output frequency: *0-1000Hz*
  - Rated output current: *4.6/4.8 A*
- **2 series connected Delta Elektronika DC power supplies**
  - Type: *SM300 D10*
  - Rated *power: 3kW*
  - Rated *current: 10A*
  - Rated *voltage: 330V*
- **2 measurement systems including**
  - LEM box for measurement of V_{dc}: *voltage transducer LV25-800, LEM*
  - LEM box for measurement of grid currents: *3 x current transducer LA55-P, LEM)*

– LEM box for measurement of grid voltages: *3 x current transducer LV25-600, LEM)*

- **Three-phase transformer**
- **dSPACE system**

7.2 Implementation of the Control System

The dSpace board features a SIMULINK interface that allows applications to be created and developed in Matlab/Simulink and the processes of compiling and automatic code generation are carried out in the background. Thanks to these features, a control system was developed in Matlab/Simulink and then automatically processed and run by the DS1103 PPC card. [23]

A Graphical User Interface (Fig. 7.3) has been build using the Control Desk software in order to allow a real time control and evaluation of the system.

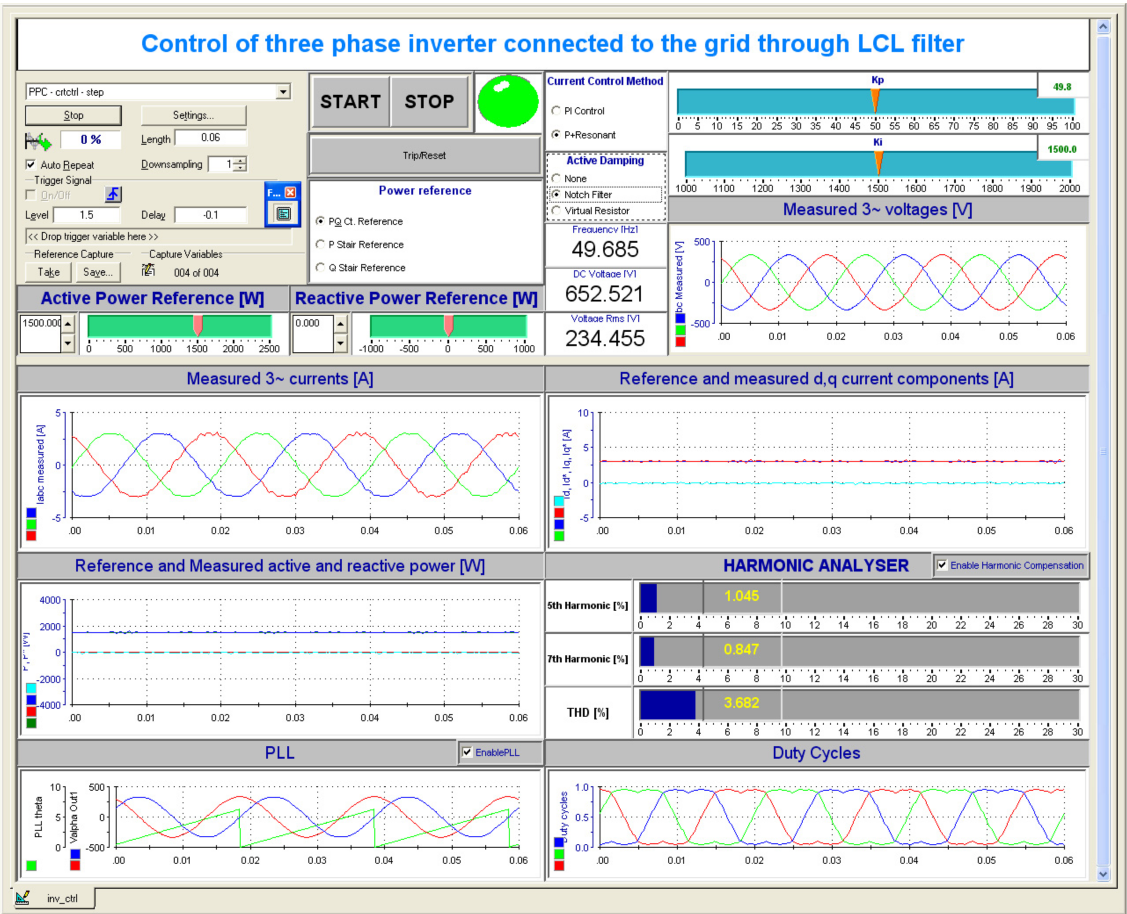

Figure 7.3: *Control Desk Graphical User Interface.*

The interface can be used to control inputs like:

- the start/stop of the system;
- active power reference;
- reactive power reference;
- current control method;
- active damping state;
- the value of the virtual resistance.

Also, it can be used to view different ouputs like:

- measured three phase grid currents;
- measured and reference d,q components of the currents;
- measured dc voltage;
- measured and reference active and reactive power;
- phase angle provided by the PLL;
- duty cycles.

7.3 Tests of the current control loop

As in the simulations, there have been chosen two experimental cases that confirm the results concerning the implementation of the current controllers. Due to time constraints, the voltage control has not been implemented, but, instead, a constant dc voltage source of 650V has been used.

7.3.1 Case 1: Steps in the active power on the system with PI current control

The reference for the active power has been varied in five steps, each with the width of 100ms. The first step is at 0.8 of the rated power, the next is at the rated power, then 0.8 again, then 0.6 of the rated power and the last is back at 0.8. The reference and the measured active power are ploted in Fig. 7.4. It can be seen that the measured power tracks very well the reference.

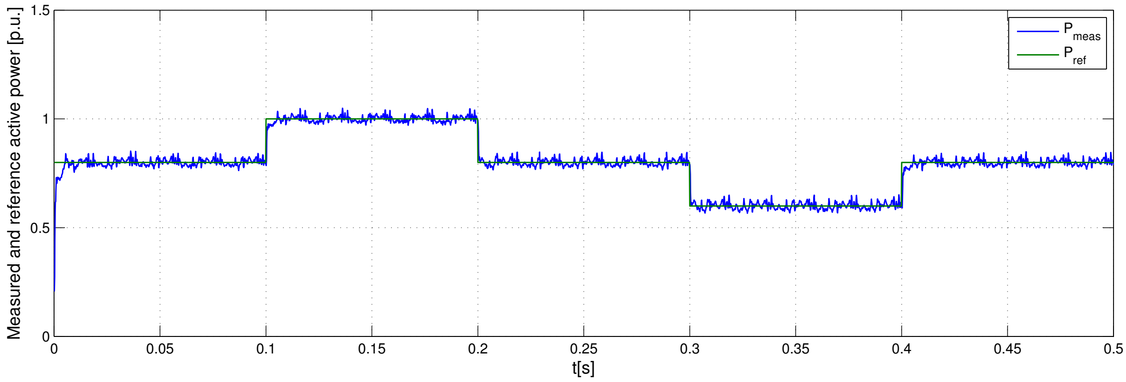

Figure 7.4: *Reference and measured active power in the experimental Case 1.*

The reactive power reference has been set to 0. The reference and the measured reactive power are plotted in Fig. 7.5.

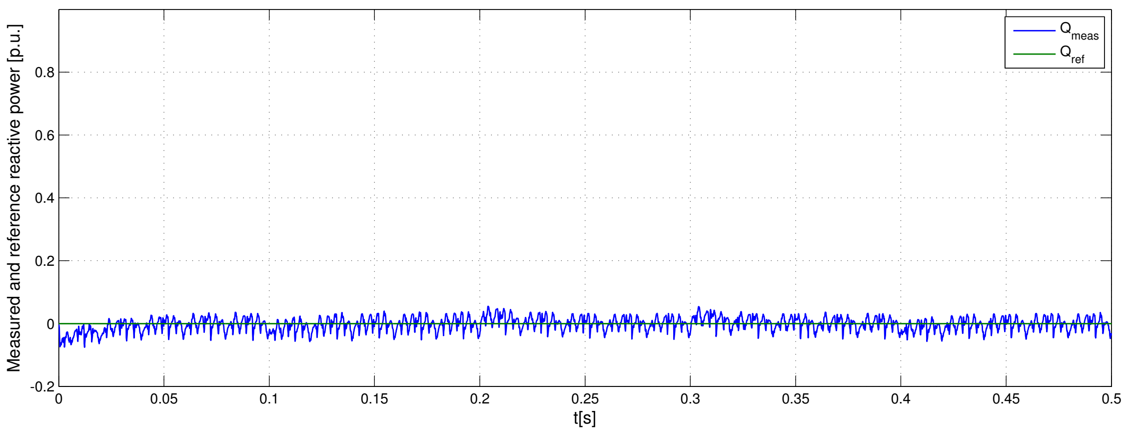

Figure 7.5: *Reference and measured reactive power in the experimental Case 1.*

The d and q components of the measured grid currents are plotted in Fig. 7.6. As i_d determines the active power, it can be seen that its reference changes proportionally with the active power, while i_q is kept at a 0 reference, given by the reactive power.

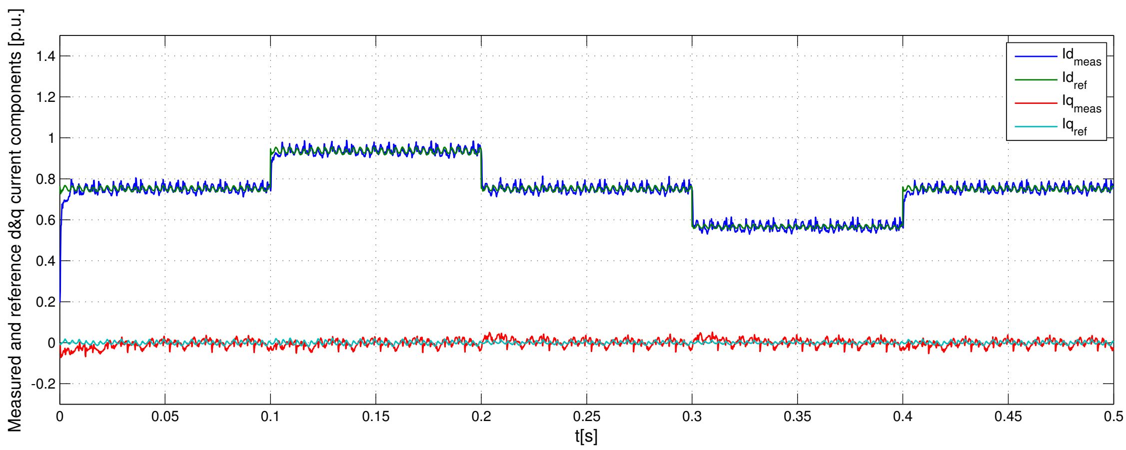

Figure 7.6: *Reference and measured d and q current components in the experimental Case 1.*

Fig. 7.7 shows the measured grid currents, as well as a zoom at the point of a step in the power reference.

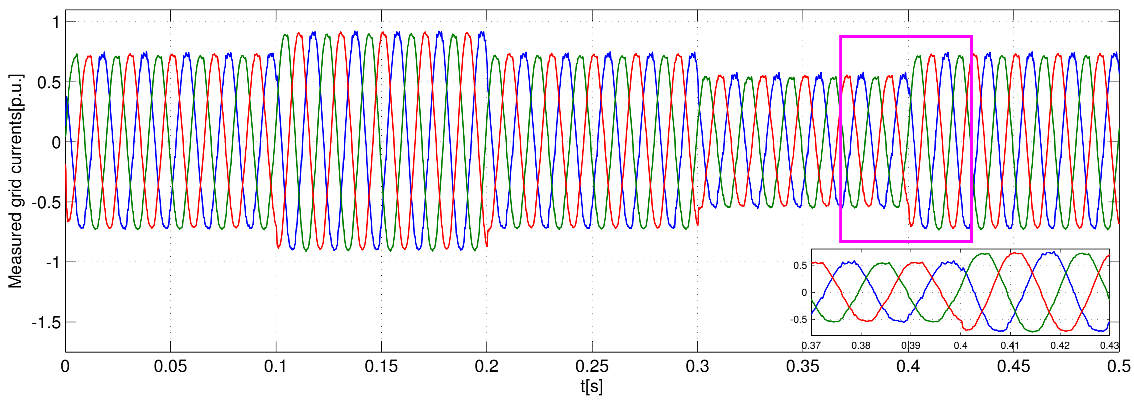

Figure 7.7: *Zoom on the measured grid currents in the experimental Case 1.*

7.3.2 Case 3: Steps in the active power on the system with PR current control

As in the experimental Case 1, the reference for the active power has been varied in five steps, each with the width of 100ms. The first step is at 0.8 of the rated power, the next is at the rated power, then 0.8 again, then 0.6 of the rated power and the last is back at 0.8. The reference and the measured active power are ploted in Fig. 7.8.

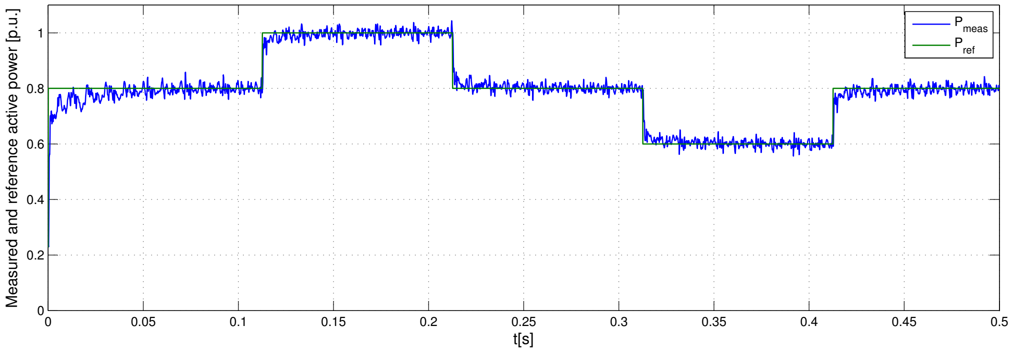

Figure 7.8: *Reference and measured active power in the experimental Case 2.*

The reactive power reference has been set to 0. The reference and the measured reactive power are plotted in Fig. 7.9.

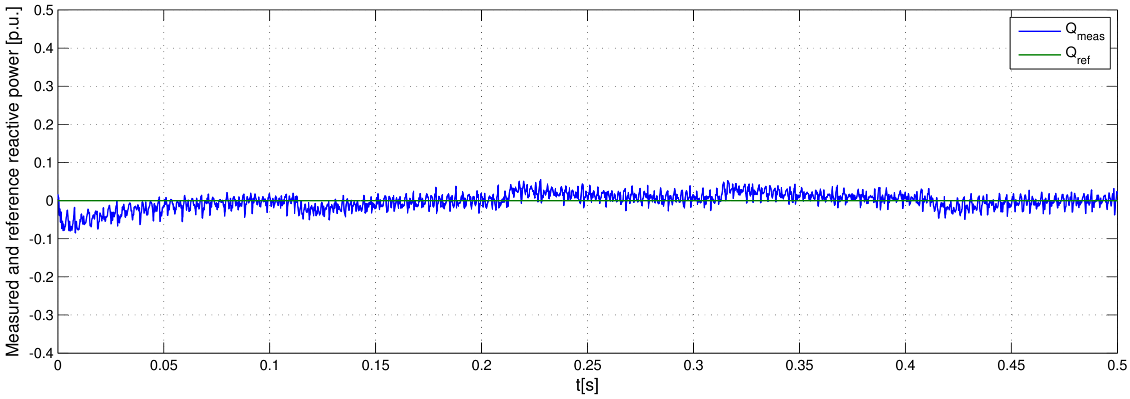

Figure 7.9: *Reference and measured reactive power in the experimental Case 2.*

Fig. 7.10 shows the measured grid currents, as well as a zoom at the point of a step in the power reference.

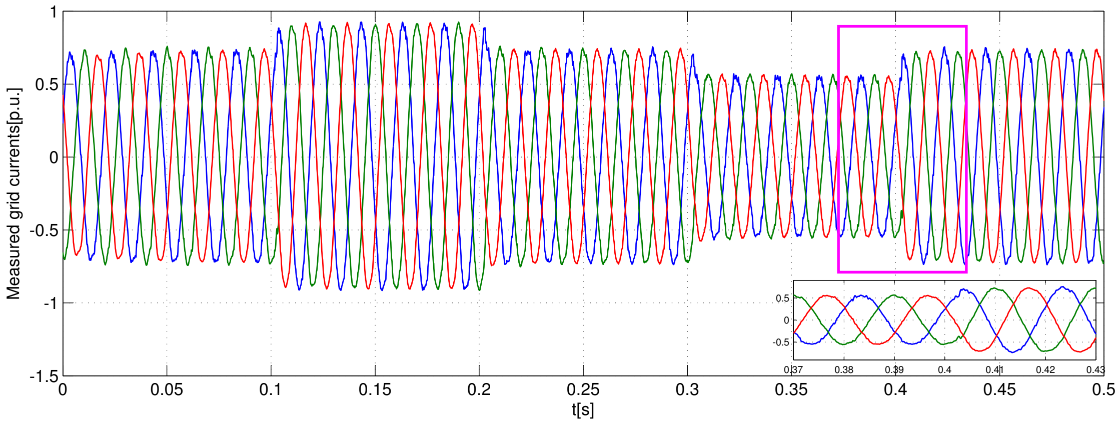

Figure 7.10: *Zoom on the measured grid currents in the experimental Case 2.*

7.4 Active Damping of the LCL filter resonance

Like in simulations, two types of tests have been implemented in the laboratory to test the behaviour of the system under the implemented active damping methods. In the first test, the proportional gain of the controller has been increased until close to the instability limit, to a value of $K_p = 55$ and the system started with no damping. After a while, the damping was switched on and then off again. This test was meant to check the efficiency of the control. In second test, a step in the current reference has been simulated, with two different values of the proportional gain, in order to show the improvement of the step response of the system as the proportional gain is allowed to be increased by active damping. This test is meant to show the robustness of the control.

7.4.1 Notch filter

In the first test performed with the notch filter, the proportional gain of the control has been set to $K_p = 55$, which is close to the instability limit for the undamped system. The Notch filter is introduced in the current loop and then taken out again. The measured grid currents are shown in Fig. 7.11.

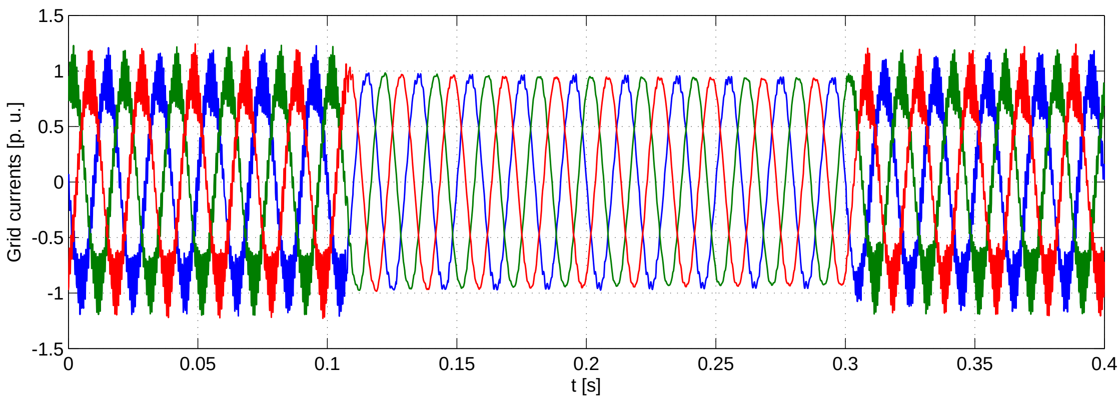

Figure 7.11: *Measured grid currents in the case of notch filter switched on and off.*

It can be seen that the currents stabilise within one period after introducing the notch filter in the system, thus proving the efficiency of the control.

In the second test, the a step in the current reference has been simulated (from 0.8 p.u. to 1 p.u.), with two values of the proportional gain. In order to be able to make a comparison between the behaviour of the undamped system and the active damping, first the step in current reference is performed on the undamped system. Fig. 7.12 shows the measured currents of the undamped system, first with a $K_p = 30$ (a) and then with a higher value, $K_p = 55$ (b) which is close to the stability limit.

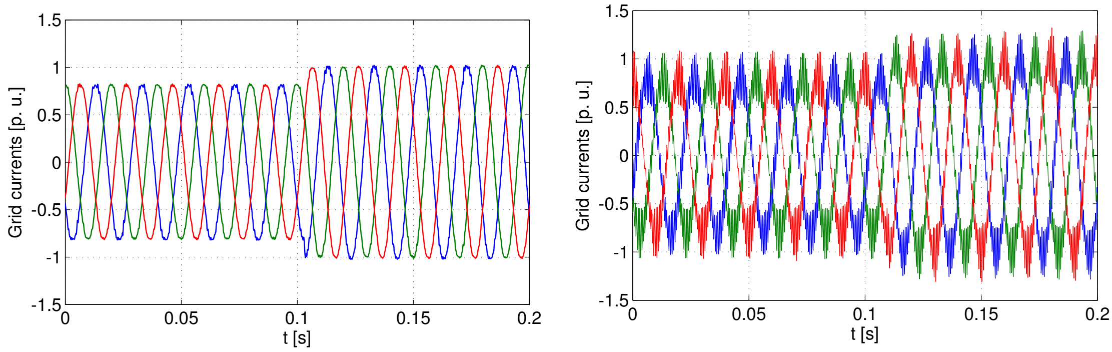

(a) Proportional gain $K_p = 30$.

(b) Proportional gain $K_p = 55$.

Figure 7.12: *Step in the current reference of the undamped system.*

A similar test has been performed on the system with a notch filter in the current loop. Fig. 7.13 shows the results, first with $K_p = 35$ (a) and then with $K_p = 55$.

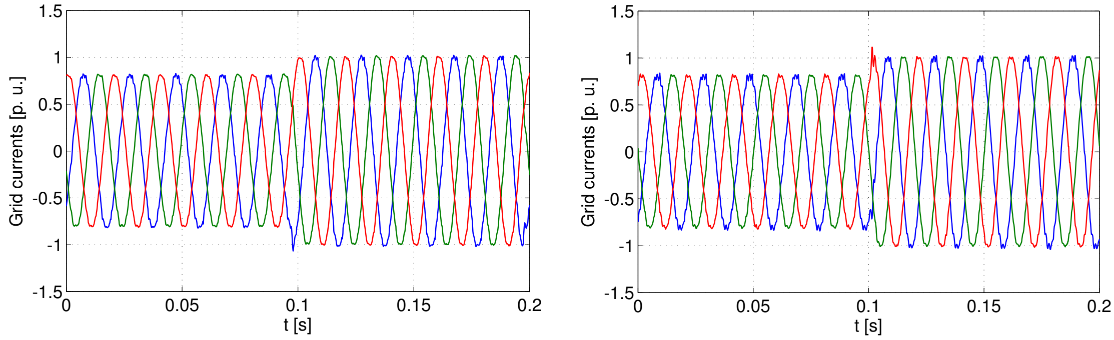

(a) Proportional gain $K_p = 35$.

(b) Proportional gain $K_p = 55$.

Figure 7.13: *Step in the current reference of the system actively damped with a notch filter.*

It can be noticed that the damped system remains stable when the proportional gain is increased, while the undamped system gets unstable.

7.4.2 Virtual resistance

The same kinds of tests have been performed to test the active damping with virtual resistance. In the first test, the proportional gain of the control has been set again at a value close to the instabilty limit, $K_p = 55$. The damping resistance is virtually introduced in the current loop in series with the filter capacitance, and then taken out again. The measured grid currents are shown in Fig. 7.14.

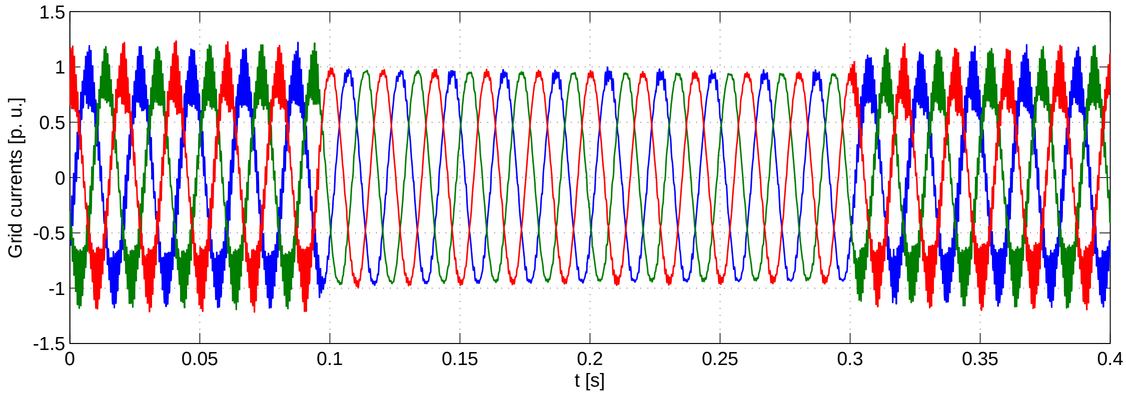

Figure 7.14: *Measured grid currents in the case of virtual resistance switched on and off.*

It can be seen that the currents stabilise within one period after virtually introducing the damping resistance in the system, thus proving the efficiency of the control.

In the second test, the a step in the current reference has been simulated (from 0.8 p.u. to 1 p.u.), with two values of the proportional gain. Fig. 7.15 shows the measured currents, first with a $K_p = 35$ (a) and then with a higher value, $K_p = 55$ (b).

Figure 7.15: *Step in the current reference of the system actively damped with virtual resistance.*

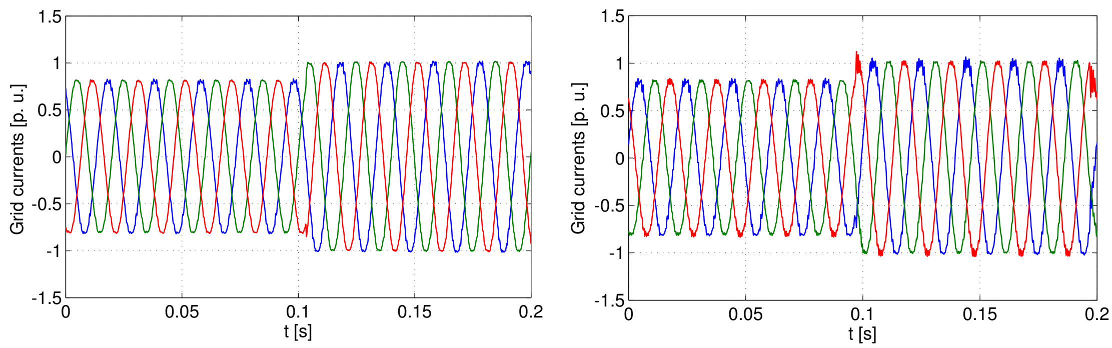

(a) Proportional gain $K_p = 35$.

(b) Proportional gain $K_p = 55$.

The plots from Fig. 7.15 show that the system shows a good step response, even when the proportional gain is increased.

8 Conclusions and Future Work

8.1 Conclusions

The main topic of this project was to study and implement different methods of active damping of the resonance frequency of an inverter connected to the grid through an LCL filter. It has been structured into 8 chapters.

In the first chapter, an introduction to the project has been made, including a short background, the project motivation and the statement of the goals.

The second chapter was a survey on the different methods to achieve damping of the resonance frequency of the LCL filter. First, the passive damping concept was described. It has been shown that, though a large resistance in the system (in series or in parallel with L_i or C_f) provides damping of the filter resonance, the power loss on the damping resistance leads to a decrease of efficiency. The three most used active damping methods were presented: the virtual resistance metod, lead-lag method and notch filter method. Each of these methods brings advantages and disadvantages. While the notch filter and the lead-lag methods require no extra sensors in the system, they are difficult to tune on the resonance frequency of the LCL filter. The virtual resistance method does not require any extra tuning computations, but, depending on the position of the virtual resistance, requires either a current or a voltage sensor.

The third chapter dealt with the filter design. First, three filter topologies were presented and explained why the LCL was the optimal choice. Then the transfer function of the LCL filter was derived and the values of the filter components were calculated, with emphasis on the resonance frequency value. Also, the root loci of the system with LCL filter was plotted at different sampling frequencies. It was shown that the sampling frequency affects the root loci of the open-loop control, and values over 4000Hz can lead the system into instability, but for a very small range of proportional gains. The sampling frequency of 3000Hz was chosen to further tune the parameters of the controller.

The next chapter was focused on the design of the control system required to control an inverter connected to the grid. A voltage oriented control has been implemented, where the active and reactive power are regulated by controlling the d and q components of the current. The chapter consists of three items that were designed: the phase-locked loop, the current loop and the dc voltage loop. Two different approaches have been considered with regard to the current loop: a 'dq' axis PI control and an '$\alpha\beta$' axis P+Resonant current control. There were some requirements imposed on the current control, regarding the phase and gain margin and, also, the bandwidth of the system. The Root Loci, Bode plots and step response graphs, plotted with the Matlab toolbox, Sisotool, have shown that the current loops (both PI and P+Resonant) fullfill the imposed requirements.

In the fifth chapter, two methods of active damping were further developed and investigated: the notch filter method and the virtual resistance method. Their frequency response was shown and their behaviour was investigated in situations like changes in grid impedance and changes in component values. It was shown that the notch filter method needs a grid detection algorithm, as the resonance frequency of the system varies a lot with the impedance of the grid, whereas the virtual resistance method was less sensitive to the changes in the grid impedance. Both methods proved to be quite robust to the changes in filter components values.

The sixth chapter presented the simulation results obtained using Matlab/Simulink. First, the current and voltage control was tested by implementing steps in the active power reference. The tests proved that both in the case of PI current control and in the case of P+Resonant current control and also for the dc voltage control, the designs of the controllers have been well performed, as the system was able to follow the power reference with good accuracy. Next, the efficiency and the robustness of the active damping methods was simulated, by switching on the active damping methods in the system initially brought close to instabillity and then simulating steps in the reference of the active power with different values of the proportional gain. Both active damping methods provided good results in simulation, bringing more stability and efficiency to the system.

In the seventh chapter, the experimental results are shown. First, the setup in the laboratory is described and the graphical interface built with ControlDesk is presented. Next, the tests performed in the labortatory are explained and discussed. The tests follow the same line as the ones carried out in simulation. First, the current controllers were tested and then the two active damping methods. The results obtained in the lab confirm the ones from simulations. Regarding the notch filter, a method of online tuning of the filter frequency was not implemented, due to the fact that the notch filter needed a discretisation method that could not be performed online. Even though a grid parameter detection algorithm was not implemented, the notch filter method provided better results with the estimated grid parameters, than the virtual resistance method, proving its efficiency and robustness.

8.2 Future work

The following items are suggested as future work for the project:

- study of active damping with virtual resistance, when the passive resistance is placed in parallel with the filter capacitance and in parallel with the inverter side inductance
- study of active damping with lead-lag element
- implementation of active damping with an adaptive notch filter, that can be tuned online at the resonance frequency of the system

- implementation of a grid parameters detection, that allows the auto-adjusting of the noch filter frequency
- using different control strategies (e.g. sliding mode control), to achieve active damping of LCL

Literature

[1] M. Liserre, A. Dell'Aquila, and F. Blaabjerg. Stability improvements of an lcl-filter based three-phase active rectifier. In *Power Electronics Specialists Conference, 2002. pesc 02. 2002 IEEE 33rd Annual*, volume 3, pages 1195–1201vol.3, 23-27 June 2002.

[2] Frede Blaabjerg, Remus Teodorescu, Zhe Chen, and Marco Liserre. Power converters and control of renewable energy systems. In *Proceedings of ICPE*, pages 2–20, 2004.

[3] Marco Liserre, Remus Teodorescu, and Frede Blaajerg. Stability of photovoltaic and wind turbine grid-connected inverters for a large set of grid impedance values. In *IEEE TRANSACTIONS ON POWER ELECTRONICS*, volume 21, January 2006 2006.

[4] M. Malinowski, M.P. Kazmierkowski, W. Szczygiel, and S. Bernet. Simple sensorless active damping solution for three-phase pwm rectifier with lcl filter. In *Industrial Electronics Society, 2005. IECON 2005. 31st Annual Conference of IEEE*, page 5pp., 6-6 Nov. 2005.

[5] Remus Teodorescu and Frede Blaabjerg. Flexible control of small wind turbines with grid failure detection operating in stand-alone and grid-connected mode. In *IEEE TRANSACTIONS ON POWER ELECTRONICS*, volume 19, pages 1323–1332, 2004.

[6] P.A. Dahono. A method to damp oscillations on the input lc filter of current-type ac-dc pwm converters by using a virtual resistor. In *Telecommunications Energy Conference, 2003. INTELEC '03. The 25th International*, pages 757–761, 19-23 Oct. 2003.

[7] P.A. Dahono. A control method to damp oscillation in the input lc filter. In *Power Electronics Specialists Conference, 2002. pesc 02. 2002 IEEE 33rd Annual*, volume 4, pages 1630–1635, 23-27 June 2002.

[8] W. Gullvik, L. Norum, and R. Nilsen. Active damping of resonance oscillations in lcl-filters based on virtual flux and virtual resistor. In *Power Electronics and Applications, 2007 European Conference on*, pages 1–10, 2-5 Sept. 2007.

[9] C. Wessels, J. Dannehl, and F.W. Fuchs. Active damping of lcl-filter resonance based on virtual resistor for pwm rectifiers &stability analysis with different filter parameters. In *Power Electronics Specialists Conference, 2008. PESC 2008. IEEE*, pages 3532–3538, 15-19 June 2008.

[10] V. Kaura V. Blasko. A novel control to actively damp resonance in input lc filter of a three-phase voltage source converter. *IEEE TRANSACTIONS ON INDUSTRY APPLICATIONS*, 33:542–550, 1997.

[11] Frede Blaabjerg Marco Liserre, Antonio Dell' Aquilla. Genetic algorithm-based design of the active damping for an lcl-filter three-phase active rectifier. *IEEE TRANSACTIONS ON INDUSTRY APPLICATIONS*, 19:76–86, January 2004.

[12] Mihai Ciobotaru. *Reliable Grid Condition Detection and Control for Single-Phase Distributed Power Generation Systems*. PhD thesis, Aalborg University, 2009.

[13] F. L. M. Antunes S. V. Araujo. Lcl filter design for grid-connected npc inverters in offshore wind turbines. *The 7th International Conference in Power Electronics*, 1:1133–1138, 22-26 October, 2007 / EXCO, Daegu, Korea.

[14] *IEEE Std. 519-1992 - IEEE Recommended Practices and Requirement for Harmonic Control in Electrical Power Systems Ű IEEE Industry Applications Society/ Power Engineering Society.*, 1992.

[15] M. Liserre, F. Blaabjerg, and S. Hansen. Design and control of an lcl-filter based three-phase active rectifier. In *Industry Applications Conference, 2001. Thirty-Sixth IAS Annual Meeting. Conference Record of the 2001 IEEE*, volume 1, pages 299–307vol.1, 30 Sept.-4 Oct. 2001.

[16] Pasi Peltoniemi. Comparison of the effect of output filters on total harmonic distotionn of line current in voltage source line converter - simulation study.

[17] Alin Raducu. Control of grid side inverter in a b2b configuration for wt applications. Master's thesis, Aalborg Universitet, 2008.

[18] A. Timbus, R. Teodorescu, F. Blaabjerg, and M. Liserre. Synchronization methods for three phase distributed power generation systems. an overview and evaluation. In *Power Electronics Specialists Conference, 2005. PESC '05. IEEE 36th*, pages 2474–2481, 16-16 June 2005.

[19] M. Ciobotaru, R. Teodorescu, P. Rodriguez, A. Timbus, and F. Blaabjerg. Online grid impedance estimation for single-phase grid-connected systems using pq variations. In *Power Electronics Specialists Conference, 2007. PESC 2007. IEEE*, pages 2306–2312, 17-21 June 2007.

[20] E. Ceanga, C. Nichita, L. Protin, and N. Cutululis. *Theorie de la Commande des Systemes*. Editura Tehnica, 2001.

[21] R. Teodorescu, F. Blaabjerg, U. Borup, and M. Liserre. A new control structure for grid-connected lcl pv inverters with zero steady-state error and selective harmonic compensation. In *Applied Power Electronics Conference and Exposition, 2004. APEC '04. Nineteenth Annual IEEE*, volume Volume 1, pages 580 – 586, 2004.

[22] M. Liserre, A. Dell'Aquila, and F. Blaabjerg. Design and control of a three-phase active rectifier under non-ideal operating conditions. In *Industry Applications Conference, 2002. 37th IAS Annual Meeting. Conference Record of the*, volume 2, pages 1181–1188vol.2, 13-18 Oct. 2002.

[23] Remus Teodorescu. *Getting Started with dSpace system*. Aalborg University.

Nomenclature

Parameters	***Description of parameters***
aw	anti-windup
C_b	base capacitance
C_{dc}	DC-link capacitance
C_f	filter capacitance
e_g	grid voltage
E_n	nominal grid line to line voltage
f	frequency
f_{sw}	switching frequency
f_s	sampling frequency
f_{res}	resonance frequency
H_{notch}	transfer function of the notch filter
H_{LCL}	transfer function of the LCL filter
$G_{PI_{crt}}$	transfer function PI current controller
$G_{control}$	transfer function of the delay introduced by the control
$G_{crt_{closed}}$	closed loop transfer function of the current loop
G_{filter}	simplified transfer function of the filter
$G_{inverter}$	transfer function of the inverter
$G_{sampling}$	transfer function of the sampling
G_{HC}	transfer function of the harmonic compensation
i^*	reference current
i_c	current through the filter capacitance
i_i	inverter side current
i_g	grid side current
i_{dc}	DC-link current
i_a, i_b, i_c	three phase currents
i_d, i_q	currents in 'dq' rotating frame
i_d^*, i_q^*	reference currents in 'dq' rotating frame
i_L	current through the inductance
i_α, i_β	currents in stationary frame
i_α^*, i_β^*	reference currents in stationary frame
i_g	current on the grid side
K_i	integral gain

K_p	proportional gain
$K_{i_{crt}}$	integral gain of the current controller
$K_{p_{crt}}$	proportional gain of the current controller
$K_{i_{vol}}$	integral gain of the dc voltage controller
$K_{p_{vol}}$	proportional gain of the dc voltage controller
L	total filter inductance
L_b	base inductance
L_i	inverter side inductance
L_g	grid side inductance
L_{grid}	grid inductance
P_d	power loss on the damping resistance
R	total filter resistance
R_{grid}	grid resistance
R_c	parasitic resistance of the filter capacitance
R_d	damping resistance
R_i	parasitic resistance on the inverter side
R_g	parasitic resistance on the grid side
s	continuous operator
$S_1..S_6$	switching states for the VSI
S_n	nominal output power of the inverter
t	time
v^*	reference voltage
v_c	voltage on the filter capacitance
v_a, v_b, v_c	three phase voltages
v_d, v_q	voltages in 'dq' rotating frame
v_d^*, v_q^*	reference voltages in 'dq' rotating frame
v_α, v_β	voltages in stationary frame
v_α^*, v_β^*	reference voltages in stationary frame
$v_g(= v_{PCC})$	grid side voltage (voltage at the PCC)
v_i	inverter side voltage
v_L	voltage on the inductance
V_{dc}	DC-link voltage
V_{dc}^*	DC-link voltage reference
Z_b	base impedance
Z_g	grid side impedance
Z_i	inverter side impedance
Z_p	impedance of the parallel filter branch
Z_{grid}	grid impedance
ω_{ff}	feed forward angular frequency
θ	grid phase angle
ψ	phase margin

Abreviations

Abreviation	***Description of abrebiation***
$DPGS$	Distributed Power Generation System
LCL	Inductance - Capacitance - Inductance
PCC	Point of Common Coupling
PI	Proportional - Integral
PLL	Phase-Locked Loop
PR	Proportional - Resonant
PWM	Pulse Width Modulation
THD	Total Harmonic Distortion
VSI	Voltage Source Inverter

Matlab/Simulink models

A

In this section, the simulation and implementation models built in Matlab/Simulink are presented.

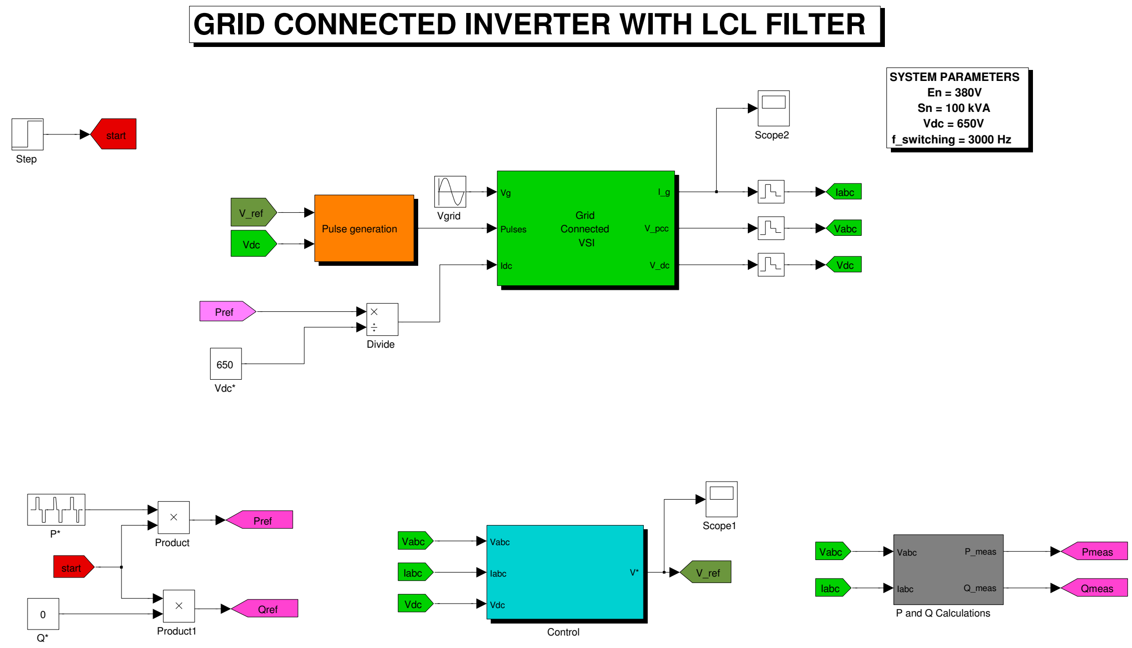

Figure A.1: *General view of the simulation model.*

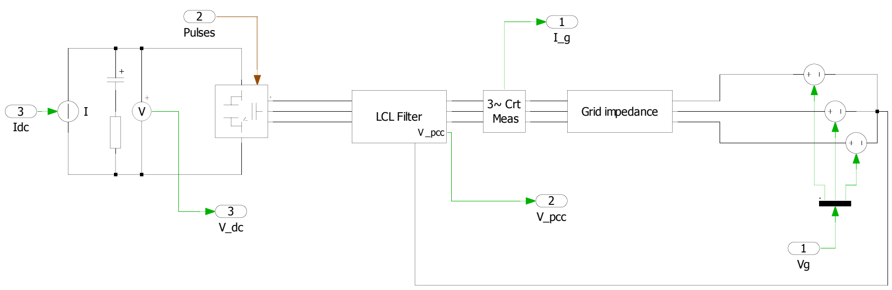

Figure A.2: *Vire of the electrical circuit built in Plecs.*

A Matlab/Simulink models

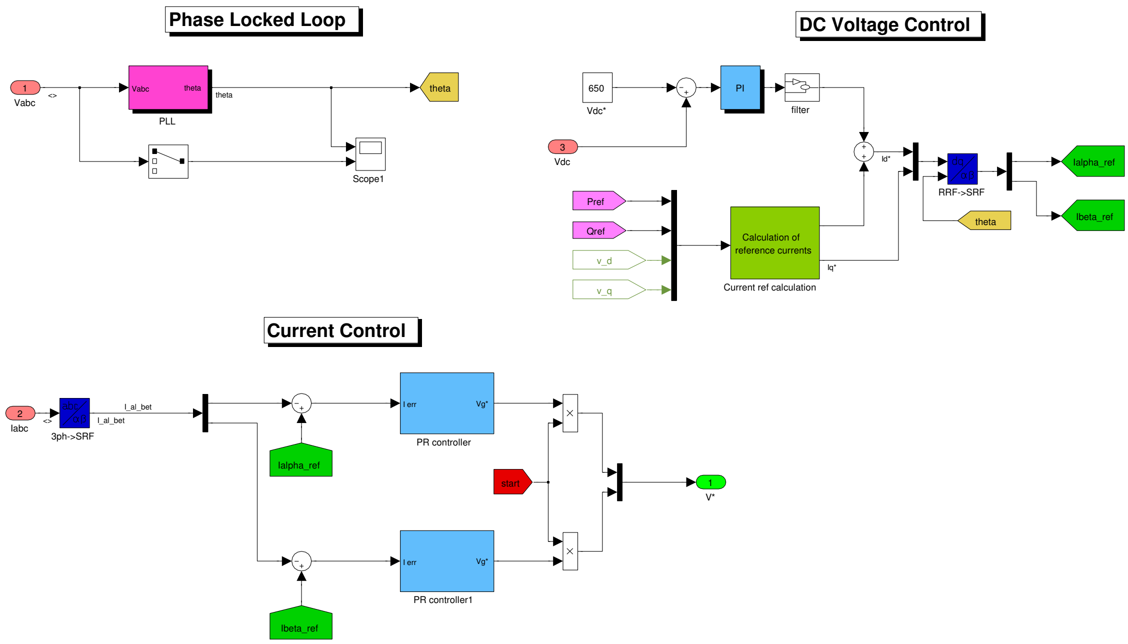

Figure A.3: *Simulink model of control.*

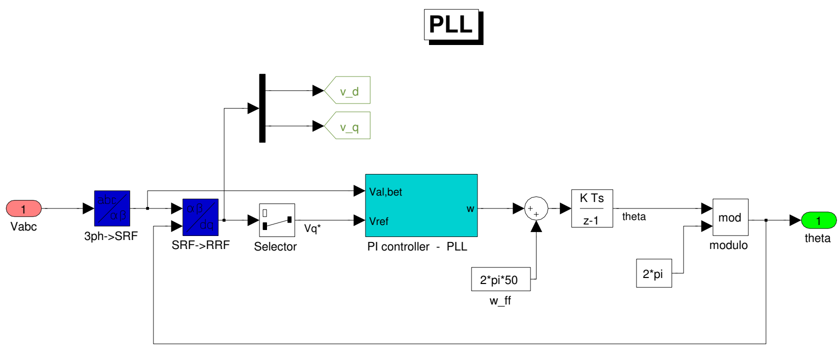

Figure A.4: *Simulink model of the PLL.*

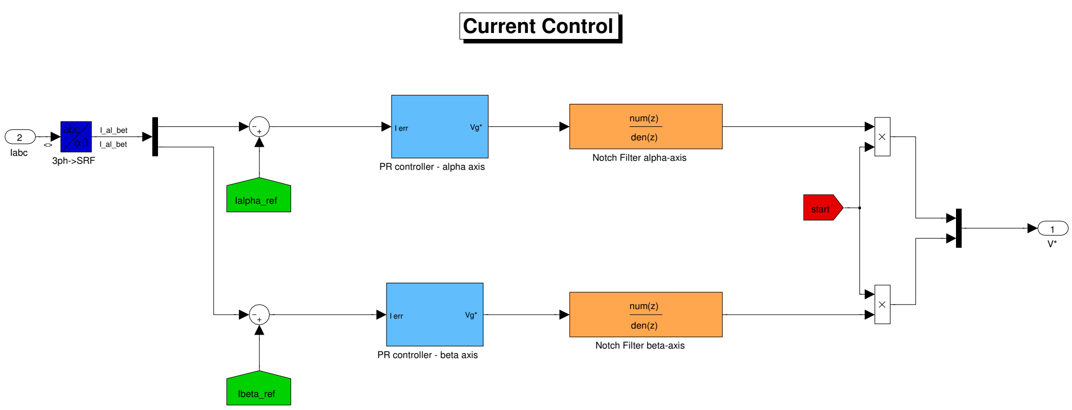

Figure A.5: *Simulink model of control with the notch filter.*

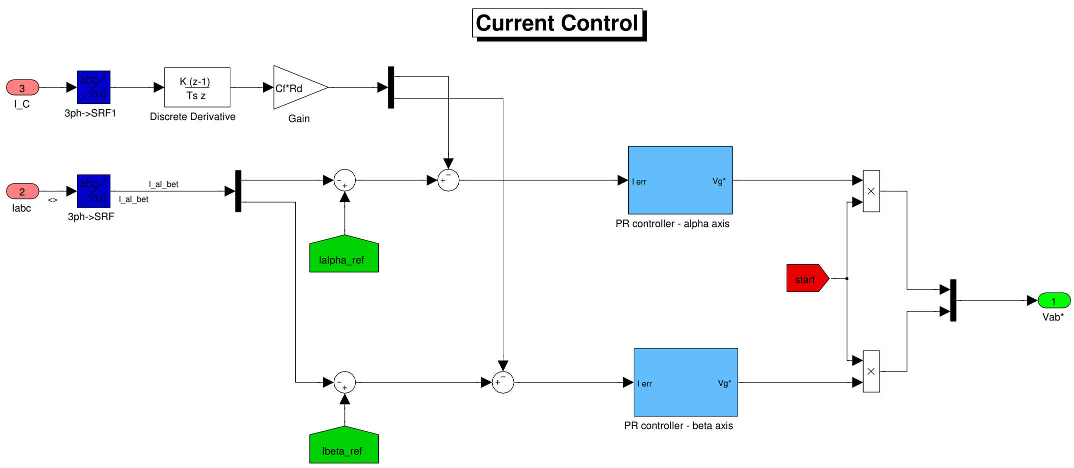

Figure A.6: *Simulink model of control with the virtual resistance.*

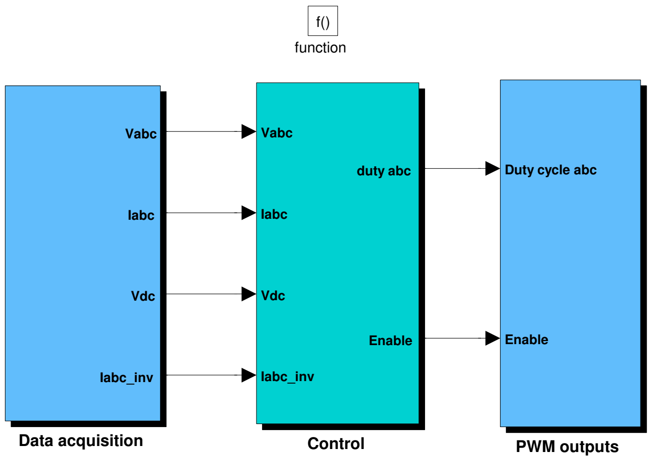

Figure A.7: *Experimental model.*

B Contents of the CD-ROM

This folder contains all articles used as references in the bibliography.

- References: This folder contains all articles used as references in this project
- Laboratory files: This folder contains the files from the laboratory implementation.
- Report files: This folder contains all source files in the Latex project file structure.
- Simulink models: This folder contains the Matlab/Simulink models used for the simulations.